JOURNAL OF PETROLOGY | VOLUME 0 | NUMBER 0 | PAGES 1–38 | 2011 | doi:10.1093/petrology/egr023

Geochemistry and Petrology of the Most Recent Deposits from Cotopaxi Volcano, Northern Volcanic Zone, Ecuador

JENNIFER M. GARRISON[1]*, JON P. DAVIDSON[2], MINARD HALL[3] AND PATRICIA MOTHES[3]

[1]DEPARTMENT OF GEOLOGICAL SCIENCES, CALIFORNIA STATE UNIVERSITY, LOS ANGELES, CA, USA

[2]DEPARTMENT OF EARTH SCIENCES, UNIVERSITY OF DURHAM, DURHAM, DH1 3LE, UK

[3]INSTITUTO GEOFÍSICO, ESCUELA POLITECNICA NACIONAL, QUITO, ECUADOR

RECEIVED APRIL 27, 2010; ACCEPTED APRIL 25, 2011

Cotopaxi volcano is located in the Northern Volcanic Zone of the South American Andes. Pyroclastic deposits and lava flows from Cotopaxi comprise basaltic andesites, andesites and rhyolites that have erupted since 13 200 years BP. Nine rhyolite eruptions were produced in at least five separate events, punctuated by intermittent andesite eruptions. High La/Yb (>5) and ^{230}Th excesses in the andesites are consistent with equilibration of magma with garnet-bearing lower crust or mantle, and numerical models show that lower crustal assimilation–fractional crystallization involving crystallization of amphibole and plagioclase is sufficient to create the observed variations in trace elements. The Cotopaxi andesites contain intergrowths of plagioclase + pyroxene, and at least four populations of plagioclase crystals indicate pervasive magma mixing. Sr, Nd and Pb isotopes are consistent with 5–20% assimilation of radiogenic crust, but higher levels of mafic crust (cryptic assimilation) and/or source contamination by volcanogenic sediments are also likely. The Cotopaxi rhyolites formed from compaction and extraction of high-SiO_2 melt from an andesitic or dacitic crystal mush. On the basis of U-series data, the residence time of the rhyolitic melts is of the order of 74 kyr. Temporal variations in MgO and Sr of the Cotopaxi andesites reflect frequent recharge of the Cotopaxi system, variable recharge composition and a system that has not become more evolved over time.

KEY WORDS: *rhyolite; lower crustal melting; subduction; U-series isotopes; igneous petrology*

INTRODUCTION

Studies of individual arc volcanoes reveal clues about process timescales, recycling of crust and, ultimately, the formation of continents. Cotopaxi Volcano is one of the more well-known volcanoes in South America, and from a geochemical perspective it provides an ideal opportunity to learn about the intricate details of the sub-volcanic magma system. Well-exposed lava flows and pyroclastic deposits allow for detailed examination of the volcanic deposits, and the stratigraphy has been well documented and calibrated by Hall & Mothes (2008). Cotopaxi has the unusual characteristic of producing both rhyolite and andesite eruptions, and the combination of this geochemical variation and calibrated stratigraphy provides a powerful tool for learning about petrogenetic processes in Ecuador over the past 13·2 kyr. Our data reveal a particularly rich record including recycling of the 2·1 Ga South American craton, repeated recharge by several andesitic magmas and the formation of rhyolite by compaction and melt extraction from an andesitic or dacitic crystal mush. The overarching goal of this work is to present a petrogenetic model for the compositional variation at Cotopaxi Volcano that takes into account the geochemical and temporal variation in the Cotopaxi andesites and rhyolites.

Geological setting

The Northern Volcanic Zone (NVZ) of the Andes (5°N–2°S) is the northernmost of four active volcanic

*Corresponding author. E-mail: jgarris@calstatela.edu

zones in South America (Fig. 1a) formed by eastward subduction of the Nazca Plate beneath the South American Plate (Lonsdale, 1978). The dip of the slab is estimated to be 25–35° (Taboada *et al.*, 2000; Guillier *et al.*, 2001) and the depth to the slab beneath the arc front is estimated to be 100–150 km (Taboada *et al.*, 2000). Volcanoes in Ecuador are distributed between two parallel mountain ranges, the Eastern and Western Cordillera (Fig. 1b), which are separated by an extensional basin called the Interandean Depression (Mamberti *et al.*, 2003). Cotopaxi Volcano (1°15'S, 78°25'W) is located in the Eastern Cordillera, ~ 60 km south of the capital city of Quito. Crustal thickness in the NVZ ranges from ~20 km near the coast to ~70 km beneath the Cordillera; in fact, with the exception of Bolivia, the lowest gravity anomaly in the entire Andean arc (−292 mgal) is beneath the NVZ (Feininger & Seguin, 1983). The crust beneath the Eastern Cordillera and the Interandean Depression consists of accreted felsic terranes and plutons that crop out as narrow belts extending northward into Colombia (McCourt *et al.*, 1984). Accreted oceanic plateau and island arc terranes, collectively referred to as the Northern Andean Block (NAB), form the basement beneath the Western Cordillera (Hughes & Pilatasig, 2002; Mamberti *et al.*, 2003; Spikings *et al.*, 2005). In southwestern Ecuador, exhumed high-grade metamorphic rocks of the Raspas Metamorphic Complex (Fig. 1b) record pressures of ~2·0 GPa and temperatures of 600°C, and may be representative of the basement beneath Ecuador (Feininger, 1980; Arculus *et al.*, 1999; Bosch *et al.*, 2002).

The most recent eruption of Cotopaxi occurred in 1877 (Wolf, 1878), and fumarolic activity on the flanks and summit of Cotopaxi suggests that there is continuing subvolcanic magmatic activity. Since 1534 Cotopaxi has experienced at least 13 andesitic eruptions (Hall & Mothes, 2008) that range from effusive lava flows to explosive strombolian and plinian style plumes. Eruptions are characterized by high eruptive power and column heights of 28–39 km (Barberi *et al.*, 1995), with estimated volumes of 0·01–8 km^3 (Hall & Mothes, 2008). Sector collapse, debris avalanches, lahars and pyroclastic flow deposits are also associated with past activity at Cotopaxi, and still pose significant hazards to surrounding communities (Mothes, 1992; Hall & von Hillebrand, 1988; Mothes *et al.*, 1998, 2004).

Stratigraphy

The Cotopaxi deposits consist of an older section called Cotopaxi I and a younger section called Cotopaxi II (Hall & Mothes, 2008) (Fig. 2a). The Cotopaxi I deposits include a series of rhyolitic pyroclastic flow and ash falls that range in age from 420 to 560 ka (fission-track ages; Bigazzi *et al.*, 1997), and are collectively called the Barrancas Sequence. These ignimbrites represent the 32 km^3 explosive eruption of the Cotopaxi Caldera, the remnant of which forms an arcuate edifice that has an estimated diameter of 8 km (Hall & Mothes, 2008). To the SE of Cotopaxi is the Chalupas Caldera (Fig. 1c), a 12 km diameter caldera that produced the Chalupas Ignimbrite 211 kyr ago (Hammersley & DePaolo, 2000; Hall & Mothes, 2008). This ignimbrite caps the Barrancas Sequence (Hall & Mothes, 2008). A 150 ka glacial till deposit separates the Cotopaxi I and Chalupas Ignimbrite from the younger Cotopaxi II sequence, which ranges in age from 13·2 ka to AD 1877 (Hall & Mothes, 2008). Lava flows related to a satellite vent on Cotopaxi, called the Morurcu vent (Fig. 1c), are found in conjunction with the glacial till deposit, and are therefore inferred to be older than 13·2 ka, but younger than 211 ka (Hall & Mothes, 2008). This study focuses on the Cotopaxi II sequence.

The Cotopaxi II sequence is subdivided into the Cotopaxi IIA (lower) and Cotopaxi IIB (upper) units; each contains pyroclastic deposits of andesite and rhyolite composition (Fig. 2b and c). The oldest Cotopaxi IIA deposits are collectively called the F-rhyolite series (Hall & Mothes, 2008), and comprise five ash fall and pyroclastic flow deposits. Two other rhyolite eruptions at 7·2 and 6·3 ka are separated from the F-series rhyolites by andesitic scoria and lava flows. The Cotopaxi IIB section comprises a series of andesitic scoria falls, lava flows and a single rhyolite eruption. The unit that separates the Cotopaxi IIA section from the Cotopaxi IIB deposits is the Colorado Canyon Ignimbrite, a 4500 year old pyroclastic flow that is well exposed on the north flank of Cotopaxi in an incised valley called the Colorado Canyon. On the basis of location and stratigraphy, this ignimbrite is presumed to have erupted from Cotopaxi Volcano; however, the Colorado Canyon Ignimbrite is geochemically and isotopically more similar to the 211 ka Chalupas Caldera Ignimbrite than to the Cotopaxi rhyolites (Fig. 2b and c). Following the Colorado Canyon eruption, Cotopaxi produced andesite (the Cotopaxi IIB series) and the Peñas Blancas rhyolite, which erupted 2200 years ago and has a composition that is consistent with the Cotopaxi rhyolites.

Widely dispersed pyroclastic deposits and lava flows, well-preserved stratigraphic exposures and an extensive, accessible ring plain allow for sampling around nearly the entire Cotopaxi cone, making it ideal for this stratigraphically controlled study. The exposures of pyroclastic deposits at Cotopaxi, which include several distinctive marker units, allow for a well-constrained volcanic stratigraphy. One consequence of the highly porous nature of vesicular pyroclasts is the increased likelihood of alteration owing to weathering; however, leached and unleached samples are not significantly different in terms of major elements, trace elements or Sr isotopes. We therefore conclude that weathering had minimal effects on rock compositions and on the outcome of this study (see Analytical Methods). Reasons for the limited alteration

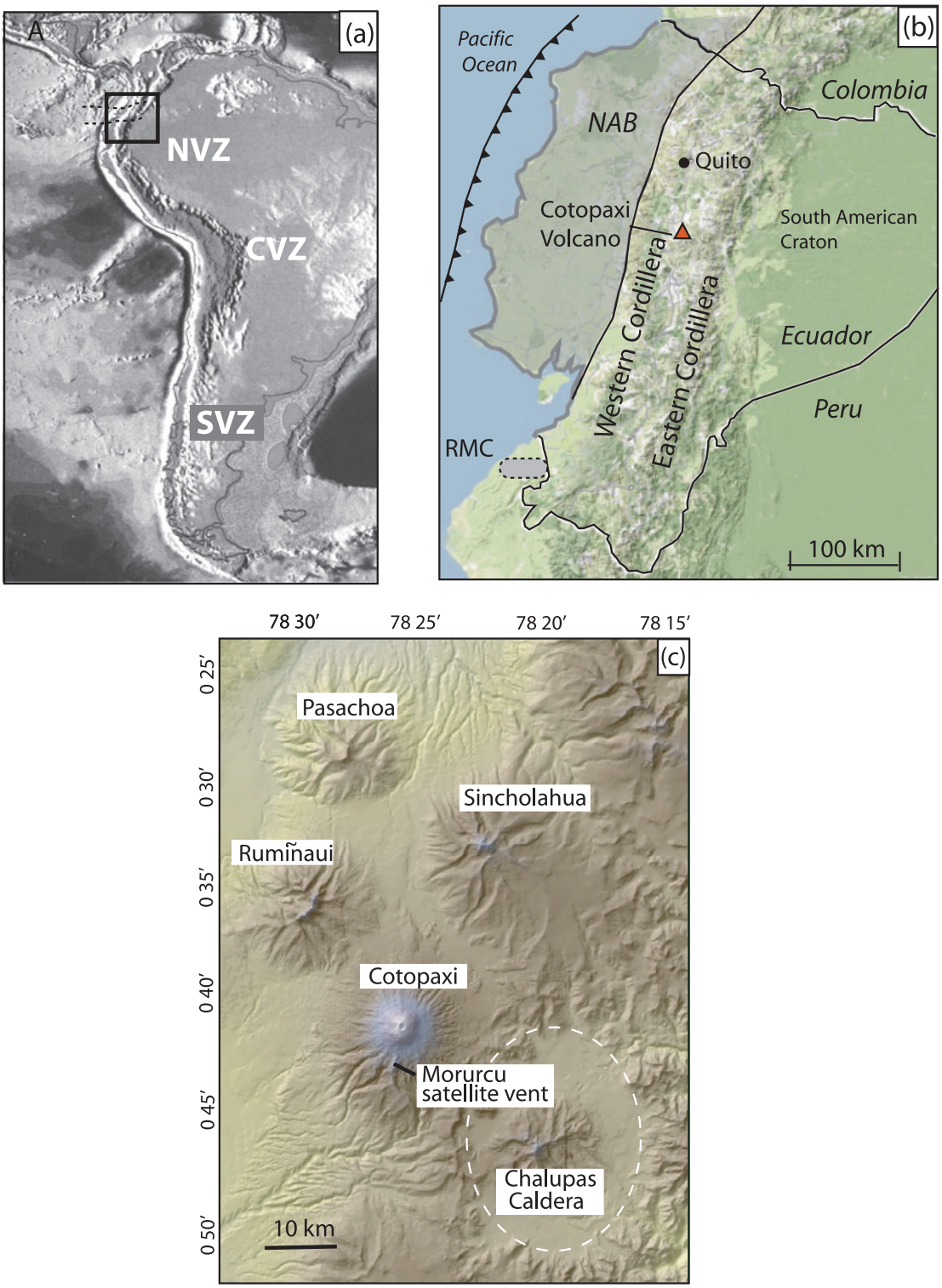

Fig. 1. (a) Location map of the study area in the Northern Volcanic Zone (NVZ) of the Andes in Ecuador, South America. The Central, Southern and Austral volcanic zones (CVZ, SVZ, AVZ, respectively) are shown for comparison. (b) Expanded region from (a) showing Ecuador and the location of Cotopaxi. The gray shaded region is the North Andean Block (NAB) (Mamberti *et al.*, 2003). RMC, approximate location of the Raspas Metamorphic Complex, from Arculus *et al.* (1999) and Bosch *et al.* (2002). (c) Digital elevation model image showing the location of the volcanoes nearest to Cotopaxi and the approximate outline of the Chalupas Caldera.

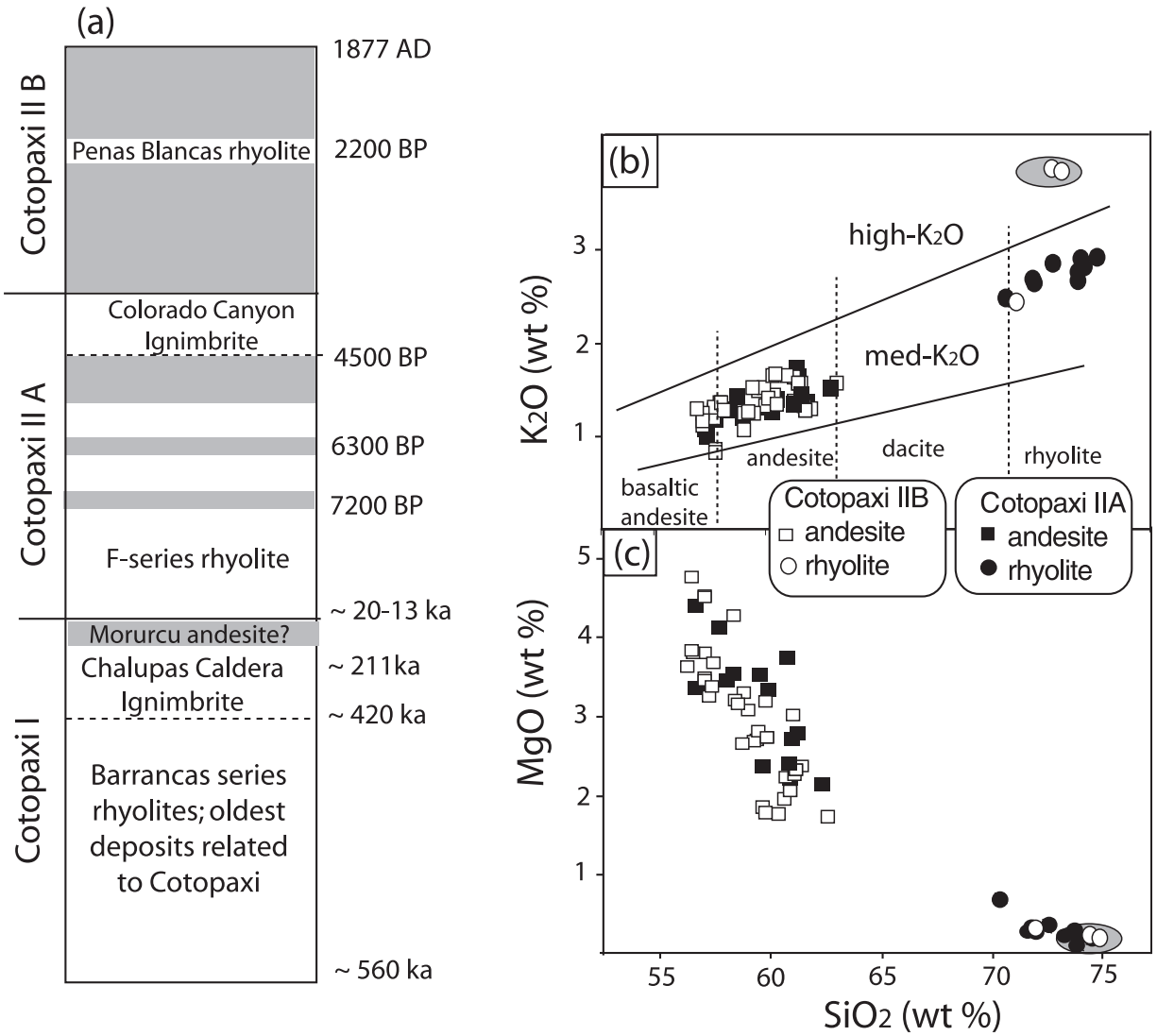

Fig. 2. (a) Generalized stratigraphic column of the Cotopaxi deposits (Hall & Mothes, 2008). Gray and white regions represent generalized andesite and rhyolite sequences. (b) wt % K_2O vs SiO_2, showing the rock name classification of LeMaitre *et al.* (1989) and (c) wt % MgO vs SiO_2 showing the compositional range of the Cotopaxi IIA and IIB sequences. The dashed lines separate the fields for basaltic andesite, andesite, dacite and rhyolite. The shaded region represents the range of Chalupas Caldera rhyolites.

may be the combination of altitude, temperature and precipitation; the ring plain of Cotopaxi is above 3630 m, and although it is cold for most of the year, the annual amount of precipitation is a fraction of what it is at lower elevations in the Amazon Basin.

ANALYTICAL METHODS

A total of 76 samples from lava flows and pyroclastic fall deposits were used for this study, collected from the flanks and ring plain of Cotopaxi, including 22 units from Cotopaxi IIA, 46 units from Cotopaxi IIB, five samples of the Colorado Canyon Ignimbrite and rhyolite from the Chalupas Caldera (Appendix Fig. A1). Metamorphic basement samples of greenschist and mica schist were collected east of the Eastern Cordillera near Banos along with three samples from the Morurcu satellite vent lavas.

All samples were ground in a ceramic shatterbox and analyzed for major and trace elements (Table 1) by inductively coupled plasma mass spectrometry (ICP-MS) and X–ray fluorescence (XRF) at Washington State University GeoAnalytical Laboratory in Pullman, Washington, using analytical techniques outlined by Knaack *et al.* (1994) and Johnson *et al.* (1999). Accuracy was determined using the standard values for AGV-1 and

Table 1: Major, minor and trace element analyses of Cotopaxi whole-rocks (in stratigraphic order)

	Cotopaxi I							
	Chalupas CTX-14	Chalupas CTX-36	Chalupas CTX-48	Chalupas CTX-86	Chalupas CTX-130	Morurcu CTX-77	Morurcu CTX-78	Morurcu CTX-82
SiO_2	72·68	73·30	73·28	73·36	71·30	62·52	60·89	61·13
Al_2O_3	13·94	13·85	14·35	13·89	14·80	17·90	18·42	18·04
TiO_2	0·237	0·24	0·25	0·23	0·26	0·661	0·696	0·604
FeO	1·22	1·25	1·32	1·19	1·35	4·96	5·52	5·43
MnO	0·04	0·05	0·05	0·04	0·05	0·09	0·09	0·10
CaO	1·22	1·15	1·23	1·20	1·23	5·46	6·22	6·33
MgO	0·24	0·31	0·31	0·28	0·34	2·23	2·47	2·77
K_2O	4·44	4·47	4·59	4·54	4·33	1·66	1·47	1·59
Na_2O	3·91	3·94	3·92	3·82	3·42	4·34	4·32	4·07
P_2O_5	0·042	0·04	0·05	0·06	0·06	0·238	0·234	0·200
Total	97·98	98·59	99·34	98·61	97·13	100·05	100·33	100·27
Ni	4	5	5	3	4	9	6	9
Cr	1	b.d.l.	1	2	3	10	19	21
Sc	2·3	2·6	2·6	2·5	2·4	11·3	13·0	
V	8	15	10	9	6	110	133	138
Ba	1056	1037	1075	1014	1056	644	578	
Rb	174·6	175·4	175·9	172·8	167·2	38·3	32·9	
Sr	223	204	213	202	187	576	609	
Zr	178	172	193	180	193	127	112	105
Y	13·32	13·28	13·70	13·54	10·24	12·62	13·39	
Nb	11·80	11·59	12·20	11·58	12·79	5·98	4·40	
Pb	18·23	22·69	15·16	23·30	25·83	8·03	5·23	
La	33·24	32·75	32·68	31·56	20·32	16·44	15·06	
Ce	56·31	55·94	55·35	54·07	38·66	31·73	28·86	
Th	23·56	22·37	23·02	22·41	19·37	3·99	3·51	
Pr	5·73	5·71	5·77	5·54	4·26	3·87	3·54	
Nd	19·37	19·65	19·86	19·36	15·15	16·29	15·12	
Sm	3·34	3·62	3·65	3·44	2·92	3·71	3·47	
Eu	0·66	0·66	0·67	0·64	0·54	1·10	1·07	
Gd	2·57	2·64	2·68	2·55	2·18	3·30	3·14	
Tb	0·39	0·41	0·41	0·40	0·33	0·46	0·46	
Dy	2·24	2·37	2·31	2·35	1·96	2·50	2·59	
Ho	0·43	0·45	0·46	0·45	0·39	0·46	0·50	
Er	1·18	1·25	1·25	1·28	1·08	1·22	1·32	
Tm	0·19	0·19	0·20	0·20	0·17	0·17	0·19	
Yb	1·23	1·29	1·27	1·31	1·12	1·04	1·13	
Lu	0·20	0·21	0·21	0·21	0·19	0·16	0·18	
Hf	5·38	5·38	5·55	5·50	5·83	3·48	3·09	
Ta	1·36	1·20	1·26	1·19	1·49	0·44	0·31	
U	9·93	9·41	9·33	9·49	7·21	1·65	1·28	

(continued)

Table 1: Continued

	Cotopaxi IIA							
	F1 AF	F2 AF	CTX	CTX	CTX	CTX	CTX	CTX
	CTX-67	CTX-17	CTX-18	CTX-61	CTX-62	CTX-66	CTX-60	CTX-65B
SiO_2	72·65	73·99	58·50	56·74	59·59	74·67	74·11	57·22
Al_2O_3	14·23	13·80	17·79	18·05	17·42	13·87	13·97	18·25
TiO_2	0·163	0·102	0·732	0·788	0·729	0·115	0·126	0·828
FeO	1·42	0·91	5·87	6·86	5·98	0·99	1·09	7·150
MnO	0·058	0·061	0·111	0·122	0·108	0·066	0·068	0·114
CaO	1·49	1·26	7·24	7·86	6·64	1·31	1·37	7·110
MgO	0·41	0·15	3·96	4·47	3·59	0·22	0·24	3·720
K_2O	2·96	3·03	1·21	1·14	1·44	3·01	2·97	1·280
Na_2O	3·98	4·32	3·94	3·89	4·11	4·26	4·34	4·090
P_2O_5	0·057	0·050	0·174	0·183	0·189	0·070	0·061	0·198
Total	97·42	97·67	99·53	100·11	99·79	98·58	98·34	99·96
Ni	11	4	17	13	17	5	5	19
Cr	34	0	79	54	82	1	0	38
Sc	3·2	2·2	19·4	22·0	18·8	2·2	2·5	24
V	18	15	161	178	142	2	3	168
Ba	954	969	523	463	589	983	920	526
Rb	71·4	74·2	27·9	25·0	33·7	74·9	71·8	29
Sr	248	229	524	549	567	215	233	599
Zr	85	84	121	113	128	91	98	110
Y	8·33	8·48	14·67	15·93	14·80	8·70	8·59	16
Nb	7·96	7·30	4·03	3·91	4·78	7·28	6·94	5
Pb	14·88	14·80	6·61	5·62	7·21	14·67	13·46	6
La	21·30	22·65	12·53	11·21	14·14	22·76	20·37	13
Ce	36·91	38·56	24·32	21·92	27·41	39·38	35·37	26
Th	8·32	9·53	3·52	2·60	3·74	8·44	8·03	3
Pr	3·85	3·99	2·96	2·78	3·33	4·16	3·78	3
Nd	13·59	13·97	12·72	12·37	14·21	14·72	13·49	14
Sm	2·53	2·42	3·12	3·17	3·42	2·67	2·52	4
Eu	0·55	0·56	1·02	1·03	1·05	0·56	0·54	1
Gd	1·94	1·88	3·08	3·07	3·16	1·98	1·88	3
Tb	0·27	0·27	0·47	0·49	0·48	0·29	0·27	1
Dy	1·50	1·46	2·69	2·89	2·83	1·56	1·53	3
Ho	0·28	0·27	0·54	0·58	0·55	0·29	0·29	1
Er	0·71	0·70	1·44	1·54	1·47	0·79	0·77	2
Tm	0·11	0·11	0·21	0·22	0·21	0·12	0·12	b.d.l.
Yb	0·72	0·70	1·29	1·41	1·30	0·76	0·76	1
Lu	0·11	0·11	0·21	0·22	0·21	0·12	0·12	b.d.l.
Hf	2·77	2·67	3·10	2·96	3·41	2·99	2·96	3
Ta	0·77	0·84	0·28	0·27	0·34	0·67	0·65	b.d.l.
U	3·89	4·03	1·31	0·93	1·40	3·47	3·38	1

(continued)

Table 1: Continued

	Cotopaxi IIA							
	CTX	F3 AF	F3 PF	F4 AF	F4 PF	CTX	CTX	CTX
	CTX-65[a]	CTX-42	CTX-43	CTX-15	CTX-19	CTX-112	CTX-109	CTX-111
SiO_2	60·61	73·86	70·53	71·90	71·84	58·41	59·76	56·71
Al_2O_3	18·95	14·88	15·49	14·80	15·13	17·15	18·18	18·44
TiO_2	0·67	0·16	0·263	0·190	0·207	0·835	0·681	0·84
FeO	5·04	1·05	1·95	1·22	1·58	6·59	5·27	7·32
MnO	0·09	0·06	0·076	0·072	0·076	0·096	0·088	0·11
CaO	6·09	1·54	2·29	1·79	2·01	6·56	5·93	7·04
MgO	1·77	0·31	0·75	0·34	0·42	3·61	2·43	3·44
K_2O	1·78	2·80	2·58	2·78	2·74	1·34	1·39	1·22
Na_2O	4·52	4·59	4·21	4·64	4·63	4·11	4·10	3·91
P_2O_5	0·23	0·07	0·101	0·078	0·093	0·235	0·218	0·19
Total	99·75	99·33	98·24	97·81	98·72	98·93	98·05	99·24
Ni	4	5	8	1	10	19	11	12
Cr	9	b.d.l.	34	1	15	89	38	18
Sc	8	2·3	4·0	2·2	2·6	14·6	13·5	18·4
V	109	4	26	14	10	151	103	170
Ba	695	1015	938	961	896	610	579	486
Rb	44	69·2	65·6	69·0	67·9	27·4	30·0	27·2
Sr	635	268	346	321	338	656	567	569
Zr	133	114	129	128	127	117	125	106
Y	16	9·03	10·03	9·61	10·00	12·43	13·73	15·67
Nb	6	7·34	6·81	6·95	6·74	5·54	5·13	4·32
Pb	9	16·25	13·52	13·39	12·85	6·87	7·59	6·00
La	17	22·03	21·00	22·03	20·80	16·44	14·93	12·72
Ce	33	37·64	37·68	38·29	36·98	31·60	28·49	25·11
Th	5	8·32	7·38	8·28	7·60	3·11	3·48	2·87
Pr	4	4·08	4·01	4·04	3·90	3·91	3·54	3·17
Nd	16	14·53	14·68	14·56	14·14	16·89	15·08	13·81
Sm	4	2·68	2·75	2·50	2·62	3·97	3·59	3·50
Eu	1	0·60	0·69	0·67	0·64	1·21	0·99	1·07
Gd	3	1·99	2·18	2·02	1·97	3·47	3·23	3·32
Tb	1	0·29	0·31	0·30	0·30	0·47	0·48	0·51
Dy	3	1·56	1·75	1·65	1·66	2·53	2·69	3·00
Ho	1	0·30	0·34	0·31	0·32	0·47	0·50	0·60
Er	1	0·79	0·92	0·84	0·85	1·18	1·28	1·59
Tm	b.d.l.	0·12	0·14	0·13	0·13	0·16	0·18	0·22
Yb	1	0·79	0·92	0·86	0·87	0·94	1·14	1·35
Lu	b.d.l.	0·13	0·15	0·15	0·15	0·14	0·18	0·21
Hf	4	3·33	3·61	3·60	3·33	3·11	3·30	2·87
Ta	b.d.l.	0·65	0·58	0·57	0·55	0·35	0·35	0·29
U	2	3·23	2·98	3·23	2·89	1·06	1·24	0·96

(continued)

Table 1: Continued

	Cotopaxi IIA							
	CTX	GF scoria[1]	GF scoria	GF lava	F5 AF	CTX	MSO[2]	MSO
	CTX-110	CTX-40a	CTX-40b	CTX-37	CTX-41	CTX-135	CTX-30	CTX-29
SiO_2	56·71	60·95	60·40	60·85		58·09	59·98	57·77
Al_2O_3	18·44	18·39	19·10	16·86		17·82	17·56	17·49
TiO_2	0·843	0·77	0·73	0·75		0·794	0·694	0·816
FeO	7·32	5·15	4·98	5·63		6·45	6·02	6·54
MnO	0·114	0·09	0·09	0·09		0·111	0·103	0·109
CaO	7·04	5·42	5·40	6·18		6·69	6·39	7·09
MgO	3·44	2·28	2·41	3·82		3·53	3·40	4·19
K_2O	1·22	1·76	1·62	1·86		1·55	1·53	1·42
Na_2O	3·91	4·11	4·12	4·24		3·82	4·03	4·00
P_2O_5	0·194	0·26	0·25	0·23		0·200	0·178	0·230
Total	99·24	99·18	99·10	100·51		99·06	99·89	99·66
Ni	12	3	3	36		16	22	35
Cr	18	7	6	95		33	58	69
Sc	17·6	13·8	13·6	17·2	3	5·6	17·6	20·0
V	170	129	131	144		165	155	162
Ba	539	757	734	759	913	932	594	594
Rb	28·6	47·3	45·2	50·1	66	95·4	36·6	32·9
Sr	612	619	643	653	386	401	518	619
Zr	106	134	134	125		114	114	118
Y	14·80	14·07	14·43	13·28	11	18·96	14·66	16·27
Nb	4·48	6·25	5·93	6·10	7	9·35	4·38	5·32
Pb	7·18	10·15	10·12	9·54	12	20·19	7·37	7·19
La	14·58	20·50	20·49	19·64	21	30·39	14·34	16·52
Ce	27·88	38·17	37·45	36·09	37	53·21	27·63	31·57
Th	3·19	5·90	6·01	5·72	7	13·32	3·95	3·93
Pr	3·43	4·56	4·56	4·31	4	6·11	3·28	3·81
Nd	14·82	18·32	18·29	17·30	15	23·10	13·78	16·12
Sm	3·59	4·15	4·20	3·79	3	4·76	3·24	3·79
Eu	1·09	1·11	1·04	1·13	1	1·09	0·95	1·13
Gd	3·19	3·46	3·30	3·19	2	3·96	3·03	3·47
Tb	0·49	0·50	0·50	0·47	0·34	0·59	0·46	0·52
Dy	2·87	2·82	2·54	2·57	2	3·40	2·66	3·02
Ho	0·55	0·53	0·57	0·47	0·38	0·67	0·53	0·59
Er	1·44	1·38	1·38	1·27	1	1·83	1·39	1·54
Tm	0·20	0·19	0·19	0·18	0·16	0·26	0·20	0·22
Yb	1·24	1·22	1·22	1·03	1	1·66	1·21	1·33
Lu	0·19	0·19	0·17	0·16	b.d.l.	0·27	0·19	0·21
Hf	2·84	3·61	3·61	3·32	4	5·42	3·01	3·07
Ta	0·30	0·43	0·43	0·41	1	0·77	0·30	0·35
U	1·11	1·83	1·86	1·70	3	4·26	1·30	1·36

(continued)

Table 1: Continued

	Colorado Canyon Series					Cotopaxi IIB		
	CC CTX-72	CC CTX-73	CC CTX-74	CC CTX-27a	CC CTX-27b	I AF CTX-16	lava A CTX-51	J PF CTX-49a
SiO_2	73·20	74·96	74·63	72·59	72·67	59·92	60·83	61·16
Al_2O_3	14·05	13·42	13·81	13·68	13·83	17·03	18·44	17·23
TiO_2	0·244	0·234	0·112	0·234	0·236	0·752	0·773	0·705
FeO	1·27	1·19	1·01	1·30	1·26	5·78	5·47	5·72
MnO	0·048	0·043	0·063	0·046	0·046	0·097	0·085	0·096
CaO	1·20	1·10	1·24	1·17	1·21	6·16	6·30	5·88
MgO	0·32	0·31	0·21	0·27	0·27	3·24	2·28	3·07
K_2O	4·70	4·16	3·07	4·58	4·58	1·56	1·49	1·68
Na_2O	3·42	3·12	4·19	3·37	3·42	4·09	4·50	4·33
P_2O_5	0·060	0·056	0·067	0·036	0·039	0·209	0·241	0·205
Total	98·51	98·59	98·40	97·27	97·56	98·84	100·41	100·07
Ni	6	6	4	4	6	10	8	18
Cr	b.d.l.	4	b.d.l.	b.d.l.	b.d.l.	47	27	55
Sc	2·4	2·4	2·1		2·2	14·5	11·8	13·1
V	11	11	10	20	10	140	125	123
Ba	1058	962	974		1052	667	647	693
Rb	173·8	153·8	79·6		163·1	36·9	29·5	41·2
Sr	204	188	206		182	569	663	569
Zr	181	175	86	174	177	123	124	125
Y	13·52	12·78	8·42		10·58	13·84	13·94	13·58
Nb	11·83	11·31	7·35		11·86	5·61	5·90	5·46
Pb	22·81	19·10	14·69		24·79	8·10	7·12	8·39
La	32·98	31·43	22·33		23·30	17·75	16·88	17·60
Ce	56·74	53·57	38·39		43·52	33·30	32·40	32·95
Th	22·47	21·47	8·55		19·44	4·80	3·31	4·87
Pr	5·83	5·56	4·04		4·58	3·95	4·01	3·93
Nd	20·15	18·91	14·41		15·89	16·21	17·14	16·46
Sm	3·63	3·46	2·63		3·00	3·74	3·97	3·78
Eu	0·69	0·65	0·54		0·54	1·14	1·19	1·11
Gd	2·67	2·58	1·91		2·22	3·31	3·49	3·28
Tb	0·41	0·40	0·27		0·35	0·49	0·49	0·49
Dy	2·36	2·22	1·53		2·02	2·67	2·68	2·73
Ho	0·45	0·44	0·28		0·40	0·50	0·49	0·51
Er	1·28	1·21	0·74		1·11	1·26	1·24	1·30
Tm	0·20	0·19	0·11		0·18	0·18	0·17	0·18
Yb	1·30	1·23	0·72		1·14	1·08	1·05	1·10
Lu	0·21	0·20	0·12		0·19	0·17	0·16	0·17
Hf	5·67	5·43	2·82		5·43	3·29	3·32	3·37
Ta	1·22	1·17	0·69		1·73	0·38	0·39	0·40
U	9·39	9·27	3·59		8·17	1·69	1·13	1·71

(continued)

Table 1: Continued

	Cotopaxi IIB							
	J AF	lava A	JK AF[3]	JK AF	CTX	CTX	CTX	CTX
	CTX-50	CTX-107	CTX-53a	CTX-53b	CTX-103	CTX-104	CTX-106	CTX-102
SiO_2	61·58	59·84	57·67	57·04	61·25	58·50	57·18	59·52
Al_2O_3	18·10	18·22	16·90	17·40	17·65	16·74	17·38	17·70
TiO_2	0·669	0·76	0·761	0·746	0·666	0·765	0·75	0·702
FeO	5·28	5·92	7·34	7·22	5·26	6·88	7·00	6·30
MnO	0·089	0·10	0·118	0·114	0·088	0·110	0·11	0·105
CaO	5·97	6·52	7·92	7·57	5·94	6·72	7·55	6·14
MgO	2·42	2·77	4·10	4·52	2·31	4·33	4·59	2·75
K_2O	1·41	1·56	0·97	0·99	1·44	1·19	0·99	1·44
Na_2O	4·48	4·29	3·77	3·92	4·32	3·84	3·62	4·15
P_2O_5	0·206	0·22	0·182	0·178	0·205	0·195	0·17	0·202
Total	100·20	100·20	99·73	99·70	99·13	99·27	99·34	99·01
Ni	10	64	28	29	8	31	30	10
Cr	26	243	77	73	26	129	80	32
Sc	13·4	14·8	23·1	22·7	12·7	17·6	22·0	14·3
V	110	123	165	177	104	163	169	136
Ba	611	607	357	387	604	507	405	592
Rb	30·0	35·0	20·9	20·7	30·7	24·5	21·3	32·7
Sr	561	593	502	497	554	532	496	551
Zr	120	121	98	95	121	108	94	118
Y	14·24	14·29	15·10	14·49	13·53	12·87	14·72	14·49
Nb	4·96	5·16	3·80	3·57	5·06	4·30	3·47	4·87
Pb	6·94	7·47	4·69	4·69	7·88	6·88	5·02	8·16
La	14·98	16·09	9·32	9·55	14·62	12·92	10·05	14·16
Ce	31·60	30·74	18·80	19·45	28·18	25·35	20·63	27·43
Th	3·30	3·79	2·23	2·14	3·12	2·55	2·12	3·29
Pr	3·62	3·75	2·45	2·47	3·47	3·16	2·61	3·40
Nd	15·23	15·86	11·30	10·97	14·76	13·82	11·82	14·56
Sm	3·70	3·79	2·90	2·95	3·59	3·44	3·13	3·57
Eu	1·03	1·12	0·94	0·94	1·06	1·00	0·94	1·03
Gd	3·26	3·40	2·94	2·94	3·17	3·11	3·07	3·29
Tb	0·49	0·51	0·48	0·46	0·49	0·46	0·47	0·49
Dy	2·69	2·81	2·66	2·72	2·68	2·60	2·79	2·79
Ho	0·51	0·54	0·57	0·53	0·51	0·49	0·54	0·53
Er	1·31	1·40	1·41	1·42	1·27	1·22	1·43	1·41
Tm	0·19	0·20	0·19	0·20	0·19	0·17	0·21	0·20
Yb	1·15	1·20	1·30	1·24	1·11	1·03	1·25	1·27
Lu	0·18	0·19	0·19	0·20	0·18	0·16	0·20	0·20
Hf	3·22	3·21	2·20	2·56	3·14	2·82	2·57	3·15
Ta	0·33	0·35	0·26	0·24	0·91	0·29	0·22	0·35
U	1·15	1·25	0·73	0·75	1·21	0·97	0·75	1·29

(continued)

Table 1: Continued

	Cotopaxi IIB							
	CTX	CTX	lava A	CTX	lava A	CTX	CTX	PB[4]
	CTX-101	CTX-99	CYX-108	CYX-96	CTX-95	CTX-98	CTX-97	CTX-90
SiO_2	58·97	61·14	59·47	57·58	57·29	58·77	56·99	68·57
Al_2O_3	17·63	18·21	17·99	18·19	19·37	17·85	17·95	15·44
TiO_2	0·764	0·702	0·76	0·83	0·69	0·70	0·87	0·278
FeO	6·68	4·82	5·84	7·28	5·39	6·73	6·78	2·06
MnO	0·109	0·082	0·09	0·12	0·09	0·12	0·12	0·081
CaO	6·62	5·93	6·46	7·00	7·84	6·53	7·21	2·55
MgO	3·36	2·01	2·80	3·48	3·20	3·06	3·99	0·69
K_2O	1·36	1·74	1·52	1·46	1·26	1·40	1·27	2·48
Na_2O	4·01	4·45	4·29	4·05	3·99	4·20	3·91	4·50
P_2O_5	0·214	0·225	0·21	0·21	0·19	0·23	0·26	0·132
Total	99·71	99·31	99·43	100·20	99·31	99·59	99·34	96·78
Ni	17	12	20					4
Cr	29	36	46					4
Sc	15·7	11·2	14·7	18·7	16·2	14·9	18·5	
V	155	105	126					17
Ba	569	688	623	608	544	578	540	
Rb	31·0	40·6	35·2	35·7	26·9	31·3	25·6	
Sr	522	620	603	610	764	605	693	
Zr	114	132	122					143
Y	14·41	15·12	14·56	15·10	11·80	15·64	14·81	
Nb	5·27	5·88	5·20	4·78	4·57	4·93	5·41	
Pb	7·78	9·35	6·39	8·23	7·32	7·52	6·32	
La	14·37	18·01	16·28	15·58	14·30	14·89	15·57	
Ce	27·91	34·19	31·14	29·81	27·10	28·99	30·53	
Th	3·08	4·38	3·83	3·98	3·41	3·14	2·94	
Pr	3·48	4·15	3·86	3·63	3·29	3·59	3·80	
Nd	14·85	17·36	16·28	15·38	13·82	15·49	16·55	
Sm	3·67	3·97	3·83	3·73	3·23	3·71	3·87	
Eu	1·06	1·17	1·17	1·10	1·05	1·10	1·18	
Gd	3·29	3·48	3·42	3·31	2·88	3·34	3·53	
Tb	0·50	0·52	0·51	0·51	0·42	0·53	0·52	
Dy	2·88	2·91	2·86	2·99	2·34	2·95	2·99	
Ho	0·53	0·56	0·56	0·57	0·44	0·59	0·55	
Er	1·36	1·47	1·46	1·46	1·11	1·50	1·44	
Tm	0·20	0·20	0·20	0·21	0·16	0·21	0·20	
Yb	1·20	1·28	1·21	1·27	0·94	1·34	1·20	
Lu	0·19	0·20	0·20	0·20	0·15	0·21	0·19	
Hf	3·09	3·57	3·24	3·02	2·58	3·11	2·93	
Ta	1·11	0·40	0·35	0·33	0·30	0·34	0·33	
U	1·19	1·51	1·27	1·31	1·09	1·17	0·97	

(continued)

Table 1: Continued

	Cotopaxi IIB							
	PB CTX-91	PB CTX-92	PB CTX-93	PB CTX-94	KA1 CTX-25	KA2 CTX-23	KB1 CTX-21	lava B CTX-47
SiO_2	61·32	60·01	61·03	73·26	59·18	59·40	57·37	59·85
Al_2O_3	17·84	17·70	18·59	14·88	18·17	18·62	18·30	17·96
TiO_2	0·679	0·697	0·71	0·16	0·795	0·732	0·822	0·77
FeO	5·23	6·16	4·40	1·05	6·19	5·55	7·13	6·07
MnO	0·091	0·103	0·08	0·06	0·108	0·100	0·111	0·10
CaO	5·99	6·10	6·01	1·54	6·42	6·66	6·90	6·46
MgO	2·38	2·78	2·10	0·31	3·14	2·74	3·31	2·90
K_2O	1·40	1·46	1·69	2·80	1·60	1·63	1·47	1·55
Na_2O	4·13	4·01	4·30	4·59	4·18	4·13	4·05	4·48
P_2O_5	0·214	0·203	0·22	0·07	0·212	0·194	0·204	0·22
Total	99·27	99·23	99·14	99·33	99·99	99·76	99·67	100·35
Ni	7	8	10·00	5	7	8	12	
Cr	27	19	20·00	0	16	21	19	
Sc	12·5	15·0	11·00	2·3	16·8	16·6	19·9	14·9
V	114	134	104·00	4	160	140	175	
Ba	585	582	659·60	1015	658	659	599	620
Rb	30·0	33·8	38·84	69·2	37·5	41·0	36·1	35·6
Sr	505	547	634·64	268	615	620	610	590
Zr	121	119	134·00	114	122	115	113	
Y	13·49	14·45	14·63	9·03	15·61	14·86	15·90	15·34
Nb	5·13	4·87	5·74	7·34	5·62	4·82	4·96	5·20
Pb	7·97	7·42	8·64	16·25	7·76	8·32	7·30	6·55
La	14·33	14·02	17·32	22·03	17·72	15·48	15·17	16·39
Ce	29·32	27·06	33·30	37·64	33·52	29·66	29·17	31·48
Th	3·22	3·43	4·36	8·32	4·53	4·67	4·07	3·96
Pr	3·46	3·34	4·00	4·08	3·98	3·55	3·52	3·89
Nd	14·68	14·36	16·75	14·53	16·78	14·78	15·14	16·77
Sm	3·59	3·47	3·88	2·68	3·89	3·38	3·57	3·97
Eu	1·01	1·02	1·13	0·60	1·16	1·04	1·08	1·18
Gd	3·25	3·22	3·40	1·99	3·43	3·10	3·31	3·55
Tb	0·48	0·49	0·51	0·29	0·51	0·47	0·50	0·53
Dy	2·77	2·80	2·89	1·56	2·96	2·65	2·83	3·03
Ho	0·50	0·54	0·54	0·30	0·56	0·52	0·54	0·57
Er	1·31	1·42	1·39	0·79	1·43	1·35	1·41	1·48
Tm	0·18	0·20	0·19	0·12	0·21	0·19	0·20	0·21
Yb	1·14	1·24	1·20	0·79	1·26	1·18	1·24	1·25
Lu	0·18	0·20	0·19	0·13	0·20	0·19	0·20	0·19
Hf	3·23	3·15	3·47	3·33	3·38	3·02	3·00	3·26
Ta	0·82	0·35	0·39	0·65	0·38	0·32	0·32	0·35
U	1·15	1·29	1·43	3·23	1·48	1·48	1·30	1·34

(continued)

Table 1: Continued

	Cotopaxi IIB							
	lava B	L unit	CTX	X unit	MZ	MZ	CTX	lava B
	CTX-46	CTX-22	CTX-24	CTX-26	CTX-34M	CTX-34Z	CTX-120	CTX-119
SiO_2	61·31	59·82	57·16	60·50	62·75	57·49	58·24	59·60
Al_2O_3	17·81	19·14	18·14	19·09	17·43	18·21	17·67	18·00
TiO_2	0·66	0·724	0·824	0·686	0·524	0·832	0·69	0·772
FeO	5·57	5·02	6·79	5·11	5·04	7·09	6·59	5·81
MnO	0·10	0·089	0·114	0·092	0·110	0·112	0·12	0·095
CaO	6·02	6·37	7·26	6·13	5·30	6·91	6·62	6·47
MgO	2·85	1·91	3·86	1·83	1·81	3·43	3·17	2·87
K_2O	1·49	1·76	1·39	1·76	1·69	1·48	1·36	1·53
Na_2O	4·27	4·37	3·95	4·39	4·16	4·01	3·95	4·22
P_2O_5	0·19	0·230	0·204	0·232	0·239	0·210	0·22	0·219
Total	100·27	99·43	99·69	99·82	99·05	99·78	98·64	99·58
Ni		2	15	2	4	9	b.d.l.	17
Cr		10	38	7	15	34		47
Sc	13·3	13·5	21·2	11·6	8·9	17·8	15·4	15·4
V		112	173	101	83	172		139
Ba	589	706	582	670	681	615	564	594
Rb	34·2	43·9	32·4	41·5	41·2	35·6	31·3	34·8
Sr	594	652	639	602	478	556	618	564
Zr		132	109	134	135	114		121
Y	13·65	16·03	15·47	15·65	15·15	15·22	15·67	14·73
Nb	4·94	5·81	4·77	5·46	5·09	4·96	4·95	5·20
Pb	6·67	8·83	6·96	8·36	9·35	8·46	6·64	7·44
La	14·31	18·22	15·17	17·41	15·96	15·94	14·50	15·76
Ce	27·77	34·99	29·32	33·33	30·24	30·54	28·03	30·09
Th	3·74	5·04	3·83	5·06	4·15	4·12	3·28	3·90
Pr	3·45	4·17	3·62	3·96	3·66	3·76	3·52	3·68
Nd	14·95	17·31	15·34	16·41	15·11	15·76	14·99	15·70
Sm	3·61	3·98	3·62	3·73	3·54	3·76	3·69	3·74
Eu	1·09	1·13	1·10	1·07	1·03	1·12	1·10	1·07
Gd	3·25	3·46	3·25	3·31	3·15	3·36	3·40	3·42
Tb	0·49	0·52	0·51	0·50	0·48	0·52	0·51	0·51
Dy	2·73	2·96	2·86	2·86	2·86	2·99	2·97	2·91
Ho	0·52	0·56	0·56	0·55	0·55	0·57	0·57	0·54
Er	1·31	1·46	1·45	1·47	1·46	1·49	1·52	1·40
Tm	0·19	0·20	0·20	0·21	0·21	0·21	0·22	0·20
Yb	1·14	1·28	1·21	1·29	1·35	1·32	1·33	1·19
Lu	0·18	0·20	0·20	0·21	0·23	0·21	0·21	0·19
Hf	3·21	3·35	2·91	3·35	3·54	3·09	3·05	3·16
Ta	0·39	0·39	0·30	0·37	0·50	0·41	0·33	0·35
U	1·62	1·61	1·19	1·63	1·47	1·33	1·16	1·30

(continued)

Table 1: Continued

	Cotopaxi IIB							
	CTX[5] CTX-116	CTX CTX-117	CTX CTX-118	CTX CTX-126b	CTX CTX-123	CTX CTX-124	lava D CTX-75	M lower CTX-20b
SiO_2	59·84	57·17	58·17	58·88	59·95	57·17	57·17	58·70
Al_2O_3	17·87	18·41	19·41	18·20	19·04	18·06	18·06	17·92
TiO_2	0·765	0·831	1·831	0·723	0·689	0·828	0·828	0·694
FeO	5·87	7·06	8·06	6·09	4·93	7·19	7·19	6·22
MnO	0·096	0·116	1·116	0·098	0·090	0·115	0·115	0·120
CaO	6·47	7·16	8·16	6·49	6·22	7·06	7·06	6·58
MgO	2·90	3·55	4·55	2·70	1·85	3·51	3·51	3·21
K_2O	1·53	1·32	2·32	1·64	1·77	1·43	1·43	1·38
Na_2O	4·22	4·03	5·03	3·94	4·22	3·90	3·90	4·14
P_2O_5	0·216	0·210	1·210	0·197	0·234	0·204	0·204	0·222
Total	99·78	99·86	100·86	98·96	98·99	99·47	99·47	99·19
Ni	19	12	13	7	3	13	13	13
Cr	44	34	35	15	9	20	20	41
Sc	15·2	17·7	18·7	15·5	12·2	18·6	14·6	15·5
V	154	171	172	149	91	179	179	137
Ba	604	571	572	667	723	588	602	508
Rb	35·4	30·2	31·2	42·6	44·2	35·6	35·2	28·0
Sr	586	656	657	604	636	617	520	550
Zr	121	112	113	118	132	111	111	112
Y	14·81	15·67	16·67	14·28	15·59	15·43	16·65	14·38
Nb	5·18	4·77	5·77	4·73	5·65	4·82	4·84	4·44
Pb	7·59	7·65	8·65	8·47	8·89	7·22	6·71	5·81
La	15·89	15·35	16·35	16·00	18·82	15·63	14·68	12·99
Ce	30·40	29·38	30·38	29·75	35·30	29·42	28·57	24·72
Th	3·83	3·41	4·41	4·69	5·17	4·06	3·58	2·87
Pr	3·73	3·64	4·64	3·54	4·18	3·54	3·57	3·09
Nd	15·92	15·54	16·54	14·97	17·58	15·33	15·42	13·36
Sm	3·79	3·83	4·83	3·50	4·01	3·68	3·72	3·23
Eu	1·13	1·17	2·17	1·03	1·17	1·13	1·12	1·03
Gd	3·39	3·47	4·47	3·16	3·43	3·33	3·51	2·97
Tb	0·50	0·53	1·53	0·48	0·53	0·51	0·54	0·45
Dy	2·91	3·05	4·05	2·69	3·03	2·90	3·07	2·56
Ho	0·56	0·59	1·59	0·52	0·59	0·57	0·62	0·50
Er	1·46	1·47	2·47	1·43	1·55	1·49	1·63	1·28
Tm	0·20	0·22	1·22	0·20	0·22	0·21	0·24	0·19
Yb	1·23	1·33	2·33	1·19	1·34	1·30	1·50	1·15
Lu	0·19	0·20	1·20	0·19	0·21	0·20	0·23	0·19
Hf	3·19	3·06	4·06	3·17	3·52	3·00	3·29	2·71
Ta	0·35	0·32	1·32	0·33	0·40	0·32	0·34	0·29
U	1·27	1·16	2·16	1·50	1·64	1·29	1·28	0·99

(continued)

Table 1: Continued

	Cotopaxi IIB							Basement[6]	
	M upper CTX-20a	CTX CTX-122	CTX CTX-125	CTX CTX-132	N scoria CTX-128	1877 BP CTX-28a	1877 BP CTX-28b	CTX 114 metapelite	CTX 115 metapelite
SiO_2	56·59	56·64	58·54	57·60	56·38	57·59	57·32	92·79	48·73
Al_2O_3	18·10	17·92	17·81	18·09	17·88	17·59	16·79	2·56	15·13
TiO_2	0·867	0·886	0·697	0·821	0·905	0·801	0·798	0·341	1·369
FeO	7·01	7·12	6·66	6·83	7·07	7·21	6·99	4·04	8·62
MnO	0·120	0·116	0·119	0·116	0·112	0·116	0·116	0·039	0·190
CaO	7·18	7·11	6·61	7·11	7·17	7·02	7·14	0·13	9·12
MgO	3·90	3·86	3·26	3·60	3·68	3·74	4·24	0·11	7·08
K_2O	1·28	1·36	1·37	1·29	1·42	1·39	1·56	0·46	0·27
Na_2O	4·05	4·02	4·01	4·21	4·10	4·02	3·89	0·24	4·45
P_2O_5	0·254	0·262	0·224	0·206	0·274	0·220	0·230	0·032	0·166
Total	99·35	99·30	99·30	99·88	98·99	99·69	99·07	100·74	95·13
Ni	20	21	15	15	18	22	22	16	103
Cr	43	36	43	29	54	37	37	92	180
Sc	19·5	17·3	15·3	17·3	15·6	18·7	18·7	2·2	35·1
V	170	157	127	169	168	164	164	19	225
Ba	560	583	545	536	621	577	577	76	120
Rb	26·3	27·2	29·0	28·8	28·3	31·5	31·5	17·1	3·1
Sr	659	695	578	633	677	614	614	16	208
Zr	112	119	116	107	124	114	114	339	91
Y	14·94	14·31	14·65	15·06	14·26	15·42	15·42	9·42	27·82
Nb	5·57	5·55	4·59	4·61	6·12	5·14	5·14	7·26	4·05
Pb	6·31	6·56	6·21	5·49	8·01	6·86	6·86	5·68	4·72
La	16·19	17·29	14·09	14·60	18·83	16·09	16·09	10·07	5·29
Ce	31·46	33·51	27·29	28·07	36·08	31·01	31·01	19·15	13·08
Th	2·94	3·37	3·11	3·26	3·55	3·76	3·76	3·59	0·59
Pr	3·79	4·10	3·36	3·48	4·40	3·73	3·73	2·12	1·94
Nd	16·52	17·60	14·50	14·82	18·85	15·84	15·84	8·09	10·03
Sm	4·00	4·11	3·54	3·60	4·29	3·72	3·72	1·76	3·45
Eu	1·20	1·22	1·08	1·11	1·27	1·14	1·14	0·33	1·50
Gd	3·41	3·55	3·14	3·29	3·64	3·43	3·43	1·56	4·26
Tb	0·51	0·51	0·49	0·51	0·52	0·51	0·51	0·26	0·79
Dy	2·94	2·92	2·83	2·86	2·89	3·00	3·00	1·59	5·04
Ho	0·55	0·55	0·55	0·56	0·53	0·57	0·57	0·34	1·05
Er	1·34	1·41	1·43	1·45	1·32	1·46	1·46	1·00	2·83
Tm	0·19	0·19	0·20	0·20	0·19	0·21	0·21	0·16	0·41
Yb	1·20	1·14	1·28	1·25	1·11	1·26	1·26	1·07	2·50
Lu	0·19	0·18	0·20	0·20	0·18	0·20	0·20	0·19	0·39
Hf	2·99	3·07	2·92	2·88	3·22	3·04	3·04	8·59	2·19
Ta	0·35	0·35	0·32	0·30	0·48	0·33	0·33	2·44	0·38
U	0·97	1·06	1·07	1·05	1·16	1·25	1·25	1·01	0·19

Samples labeled a and b are leaching experiments used to test for alteration. Both samples a (leached) and b (non-leached) are shown for comparison for several samples (with the exception of 20a and b, which are layers within the same unit). Major elements and Ni, Cr, V and Zr were measured by XRF; all other trace elements were measured using ICP following the methods established by the GeoAnalytical Lab in Pullman, WA. b.d.l., below detection limit

[1]GF is a regional marker unit.

[2]MSO, Mariann Smith outcrop; soil dated here at 4420 ± 80 years BP.

[3]Soil above this unit dated at 2050 ± 80 BP.

[4]PB, Penas Blancas; location is shown in Fig. A1.

[5]Samples 116–124 were collected beneath Yanashatcha D-type lava flow.

[6]Basement samples were collected near Tungurahua Volcano, north of Banos.

G-2. Precision was determined using internal standards BCR-P and GSP-1, and is better than 1% for the major elements, 5% for the rare earth elements (REE) and 10% for all the other trace elements. A representative subgroup of samples was chosen for $^{87}Sr/^{86}Sr$ ($n = 50$), $^{143}Nd/^{144}Nd$ ($n = 38$) and $^{206}Pb/^{204}Pb$, $^{207}Pb/^{204}Pb$, $^{208}Pb/^{204}Pb$ ($n = 16$) analysis (Table 2), by thermal ionization mass spectrometry (TIMS) on a VG Sector instrument at the W. M. Keck Center for Isotope Geochemistry at UCLA. Accuracy was monitored using standards, for which we determined $^{87}Sr/^{86}Sr = 0{\cdot}710258 \pm 10$ for NBS-987 ($n = 14$) and $^{143}Nd/^{144}Nd = 0{\cdot}511852 \pm 12$ for La Jolla ($n = 10$). Pb isotope fractionation correction was achieved by determining the value for the NBS 981 standard relative to the accepted value of $16{\cdot}937 \pm 12$ for $^{206}Pb/^{204}Pb$ ($n = 6$), $15{\cdot}491 \pm 12$ for $^{207}Pb/^{204}Pb$, and $36{\cdot}549 \pm 12$ for $^{208}Pb/^{204}Pb$, resulting in fractionation corrections of 266, 301 and 321 ppm, respectively.

Meticulous removal of weathering rinds during sample processing helped minimize the effect of alteration. To determine the effects of weathering on the pyroclastic rocks, a group of samples representing various compositions were leached for several hours in dilute nitric acid prior to analysis. After leaching, the leached and non-leached samples (designated as a and b in Table 1) were dried and prepared for analysis. There was no significant difference between leached and unleached samples, and we are confident that magmatic compositions have not been compromised by weathering.

U-series isotopes (U and Th) for whole-rocks and mineral separates were analyzed at Bristol University, UK [analytical details have been given by Garrison *et al.* (2006)]. Minerals for oxygen isotope analysis (Table 3) were separated using heavy liquids, leached in dilute hydrofluoric acid, then hand-picked to ~98% purity. Oxygen isotopes were measured for two rhyolites (CTX-17 and 19) and three andesites (CTX-25, 26 and 129) using the Optima mass spectrometer at Royal Holloway University of London, using the Gore Mountain Garnet (GMG) as a standard ($\delta^{18}O = 5{\cdot}78 \pm 0{\cdot}2$).

Zircon crystals were separated from the most evolved Cotopaxi rhyolite (CTX-17, $n = 7$) and from the Chalupas Caldera rhyolite ($n = 12$) and their U–Pb ages determined using the method of Dalyrmple *et al.* (1999) and the AS-3 standard. All zircon analyses were carried out using the Cameca IMS 1270 ion microprobe at the W. M. Keck Center for Isotope Geochemistry at UCLA. Prior to analysis, zoning in the grains was imaged using a LEO 1430VP scanning electron microscope cathodoluminescence (CL) detector, also at UCLA. Modal abundances of minerals in thin section were determined by point counting. Mineral and glass compositions were determined using a JEOL JXA-8200 electron microprobe at UCLA. Mineral composition data are given in Supplementary Data Table A1 (available for downloading at http://www.petrology.oxfordjournals.org). Further details of sample locations and preparation have been given by Garrison (2004).

RESULTS

Petrography

The Cotopaxi II lava flows [referred to as lavas A, B and D by Hall & Mothes (2008)] contain 48–23% crystals; the groundmass contains abundant microphenocrysts of plagioclase that give rise to trachytic textures. Of the phenocrysts, plagioclase accounts for 80–85%, and clinopyroxene and orthopyroxene account for roughly equal percentages of 7–10% each (Appendix Fig. A2). Accessory ilmenite and magnetite form ~1% of the lavas. The scoria clasts range from moderately to highly vesicular (25–60% vesicles) and contain 70–92 modal % groundmass, including microphenocrysts of plagioclase. Plagioclase also forms 75–90% of the phenocryst population, whereas 10–20% of the phenocrysts are orthopyroxene, which decreases with increasing SiO_2 content (Appendix Fig. A2). Clinopyroxene forms the remaining 8–20%, and the abundance is positively correlated with wt % SiO_2. At least four populations of plagioclase phenocrysts are observed in the lavas and pyroclastic deposits: those with resorbed cores, resorbed rims, whole crystal resorption and no resorption (pristine crystals) (Fig. 3a–d). Melt inclusions are observed in many plagioclase crystals (Fig. 3e). All of the analyzed mafic rocks contain clinopyroxene and orthopyroxene, either as intergrowths (Fig. 3f) or as pristine crystals (Fig. 4a and b). Olivine is found as inclusions in orthopyroxene (Fig. 4c). The Morurcu lavas contain ~25–48% crystals, primarily amphibole and plagioclase, with sparse clinopyroxene. The amphibole in the Morurcu samples is severely resorbed and does not appear to be in equilibrium with the groundmass (Fig. 4d).

The Cotopaxi rhyolites contain only 2–4% phenocrysts, including plagioclase, biotite, amphibole and trace amounts of quartz, oxides, apatite, allanite and zircon. Unlike the plagioclase crystals from the andesites, the rhyolite plagioclase crystals are pristine, show normal zonation and are commonly broken (Fig. 4e). The pyroclastic flow deposits contain obsidian and volcanic lithic fragments in the matrix, and the pumice clasts are white, fairly dense and non-fibrous. This is in contrast to pumice clasts from the Chalupas Ignimbrite, which are gray in color, glassy, highly fibrous and contain 1–2% plagioclase and biotite crystals, with accessory apatite and oxides. The Colorado Canyon rhyolite pumices have the same texture and mineralogy as the Cotopaxi rhyolite. Amphibole is observed only in the least evolved rhyolite; it is pristine and lacks alteration rims (Fig. 4f). Plagioclase crystals from the Cotopaxi rhyolite range in composition from

Table 2: Cotopaxi Sr, Nd and Pb isotope data*

Sample	$^{87}Sr/^{86}Sr$	$2\sigma \times 10^{-5}$	Sr (ppm)	$^{143}Nd/^{144}Nd$	$2\sigma \times 10^{-5}$	Nd (ppm)	$^{208}Pb/^{204}Pb^*$	2σ	$^{207}Pb/^{204}Pb^*$	2σ	$^{206}Pb/^{204}Pb^*$	2σ	Pb (ppm)	SiO_2 (wt %)
Rhyolite														
CH 99-14	0·70443	10	223	0·51282	10	19·4	38·825	0·005	15·650	0·004	18·981	0·004	18·2	72·7
CTX 99-15	0·70419	11	321	0·51282	9	14·6								71·9
CTX 99-17	0·70424	10	229	0·51281	9	14·0								74·0
CTX 99-19	0·70418	11	338	0·51286	10	14·1	38·650	0·005	15·602	0·005	18·932	0·004	12·9	71·8
CTX 99-60	0·70424	10	233			13·5								74·1
CTX 99-66			215			14·7	38·762	0·004	15·640	0·003	18·970	0·003	14·7	74·7
CTX 99-67							38·644	0·008	15·600	0·008	18·933	0·007		
CC 99-27B	0·70440	13	224	0·51272	10	19·2								72·7
CTX 99-35	0·70440	13	210	0·51276		19·8								73·7
CTX 99-36	0·70446	10	217	0·51284	7	22·1	38·781	0·005	15·639	0·004	18·968	0·004	24·2	73·3
CTX 99-42	0·70421	11	268	0·51279	17	14·5								73·9
CTX 99-69			230	0·513	7	14·8								74·2
CTX 99-72			204			20·2	38·769	0·007	15·627	0·007	18·962	0·007	22·8	73·2
Andesite														
CTX 99-16	0·70426	15	569	0·51280	12	16·2								59·9
CTX 99-18	0·70408	15	524	0·51285	11	12·7								58·5
CTX 99-20A	0·70418	10	659	0·51286	12	16·5	38·823	0·008	15·654	0·007	18·955	0·006	6·3	56·6
CTX 99-20B	0·70410	11	550	0·51285	9	13·4								58·7
CTX 99-21	0·70416	11	610	0·51288	10	15·1								57·4
CTX 99-22	0·70413	13	652	0·51280	11	17·3								59·8
CTX 99-23	0·70417	10	620			14·8								59·4
CTX 99-24	0·70417	11	639	0·51282	9	15·3								57·2
CTX 99-25	0·70411	9	615	0·51282	11	16·8								59·2
CTX 99-26	0·70410	9	602	0·51252	9	16·4	38·696	0·013	15·617	0·010	18·923	0·008	8·4	60·5
CTX 99-28B	0·70415	11	614	0·51281	11	15·8	38·737	0·010	15·617	0·015	18·937	0·012	6·9	57·6
CTX 99-29	0·70415	11	619	0·51283	12	16·1	38·664	0·006	15·608	0·005	18·907	0·004	7·2	57·8
CTX 99-30	0·70415	11	518			13·8								60·0
CTX 99-31	0·70412	11	636			20·6								55·9
CTX 99-34Z			594				38·678	0·005	15·614	0·005	18·827	0·005	9·0	57·5
CTX 99-37	0·70422	10	653	0·51275	8	17·3								60·9
CTX 99-39	0·70414	11	443			16·6								68·4
CTX 99-40A	0·70423	18	629	0·51278	12	18·4								61·0
CTX 99-40B			406	0·51282	10	15·4								71·2
CTX 99-41	0·70417	11	386	0·51282	8	15·4								
CTX 99-46	0·70409	11	594			15·0								61·3
CTX 99-47	0·70415	10	590	0·51284	10	16·8								59·9
CTX 99-49A	0·70420	10	569	0·51281	7	16·5								61·2
CTX 99-49B	0·70419	10	573	0·51280	9	16·5								61·4
CTX 99-50	0·70414	11	561	0·51283	7	15·2								61·6
CTX 99-51A	0·70416	10	663	0·51283	8	17·1								60·8
CTX 99-53A			499	0·51285	16	11·1								57·2
CTX 99-53B			497	0·51283	10	11·0	38·699	0·007	15·626	0·006	18·944	0·005	4·7	57·0
CTX 99-74			206			14·4	38·811	0·005	15·651	0·005	18·979	0·005	14·7	74·6
CTX 99-79	0·72522	11	62			19·6						6·7		78·8
CTX 00-132							38·655	0·005	15·610	0·004	18·917	0·004		
Basement samples														
CTX 00-114	0·72675	11	19											92·8
CTX 00-115	0·70422	14	211				38·442	0·005	15·577	0·005	18·995	0·005	3·0	48·7

*Pb isotope ratios are corrected for mass fractionation.
Analyses were conducted using the VG Sector 54 TIMS at UCLA. The standard values for NBS-987 (Sr), La Jolla (Nd) and NBS 981 (Pb) were used to determine accuracy. The Pb ratios are not double-spiked.

Table 3: Cotopaxi mineral oxygen isotope data

Sample	$\delta^{18}O_1$ (‰)	$\delta^{18}O_2$ (‰)	$\delta^{18}O_{avg}$ (‰)	SD
CTX 99-17				
magnetite	3·02	2·48	2·75	0·54
biotite	6·47	6·63	6·55	0·16
plagioclase	7·26	7·26	7·26	0·00
glass	8·83		8·83	–
whole-rock*			8·27	
CTX 99-19				
magnetite	3·39	3·21	3·30	0·18
amphibole	6·37		6·37	–
plagioclase	7·33	7·16	7·25	0·17
glass	6·44	6·20	6·32	0·24
whole-rock*			6·42	
CTX 99-42				
biotite	6·64	6·80	6·72	0·16
plagioclase	7·33	7·54	7·44	0·21
CTX 99-25				
magnetite	4·10	4·00	4·05	0·10
pyroxene	6·54	6·45	6·50	0·09
plagioclase	6·60	6·68	6·64	0·08
glass	7·26	7·33	7·30	0·07
whole-rock*			6·75	
CTX 99-26				
magnetite	4·89		4·89	–
pyroxene	6·38	6·22	6·30	0·16
plagioclase	6·49	6·65	6·57	0·16
glass	8·01	7·94	7·98	0·07
whole-rock*			6·93	
CTX 00-129				
magnetite	4·07	4·25	4·16	0·18
pyroxene	6·31	6·42	6·37	0·11
plagioclase	6·91	7·05	6·98	0·14
glass	7·25	7·03	7·14	0·22
whole-rock*			6·85	
CTX 99-28				
magnetite	5·68		5·68	–
pyroxene	6·16	6·22	6·19	0·06
plagioclase	6·63	6·53	6·58	0·10
glass	6·58		6·58	
whole-rock*			6·49	
Gore Mt. Garnet	($n = 15$)		5·57	0·299

Samples CTX-17, CTX-19 and CTX-42 are rhyolites, the remaining samples are andesites. Analyses were conducted by laser fluorination at University College, London. Gore Mountain Garnet (GMG) and San Carlos olivine (SC) were used as standards.
*Calculated using mineral and glass percentages, and the corresponding $\delta^{18}O$ values. Mineral percentages are given in Fig. A2.
$\delta^{18}O_1$, first measurement, $\delta^{18}O_2$, repeat value, av., average.

An_{27} to An_{52}, whereas plagioclase crystals in the andesites range from An_{50} to An_{80} (Fig. 5a; Supplementary Data Table A1), with no consistent relationship between core and rim compositions. Clinopyroxene crystals that are found in some of the rhyolites have the same composition as clinopyroxene found in the andesites (Fig. 5b).

Geochemistry

Major and trace elements

Major and trace element data are presented in Table 1. The Cotopaxi samples comprise medium K_2O basaltic andesites, andesites and rhyolites, whereas the Chalupas and Colorado Canyon ignimbrites are high-K_2O rhyolites (Fig. 2b). Major elements define differentiation trends that are characteristic of subduction-related volcanic rocks; the basaltic andesites and andesites show decreasing FeO, MgO (Fig. 2c), CaO, Al_2O_3 and TiO_2 with increasing SiO_2 that typically reflects fractionation of plagioclase + pyroxene + oxides ± olivine. K_2O and Na_2O are positively correlated with SiO_2. The SiO_2 content of glass in the andesite groundmass ranges from 61 to 78%, higher than the correlative andesite whole-rocks (55–60 wt %), and the K_2O content of the andesite glass ranges from 1·5 to 3·0 wt %, compared with whole-rock values of 1·2–1·8 wt % (Fig. 6, Table A1). The Cotopaxi rhyolites have higher concentrations of K_2O (Fig. 2b) and Na_2O than the andesites, and P_2O_5 is negatively correlated with SiO_2 content. The rhyolite glass contains 72–76 wt % SiO_2, 1–3 wt% higher than the rhyolite whole-rocks, whereas the K_2O content in the rhyolite glass is 1·9–2·7 wt % lower than in the whole-rocks.

Incompatible trace element (ITE) and rare earth element (REE) patterns for the Cotopaxi rocks are shown in Fig. 7a–c. All samples show characteristics that are typical of subduction zone volcanic rocks, including relative Ta–Nb depletions and enrichment in the large ion lithophile elements (LILE) and light rare earth elements (LREE) compared with the heavy rare earth elements (HREE). The Ta–Nb depletion in arc lavas is presumed to be a characteristic of the source that reflects the relatively low fluid mobility of Ta and Nb (Schmidt *et al.*, 2004), or alternatively, the sequestering of Ta and Nb in a residual mantle phase (Tiepolo *et al.*, 2000). The enrichment in the LILE and LREE concentrations, including K, U, Sr, Ba, Th, Pb and La, is attributed to a slab fluid component as well as to the relative incompatibility of these elements during crystallization (Davidson, 1996; Hawkesworth *et al.*, 1997). Relative depletions in the HREE are commonly illustrated using LREE/HREE (Fig. 7c), specifically La/Yb or La/Lu. Values of La/Yb > 5 are considered to be fractionated; the Cotopaxi andesites are in the range of 7–19 in the andesites and 25–35 in the rhyolites. Similarly, fractionation between the LREE and middle REE (MREE) is shown using La/Dy; values are lower in the

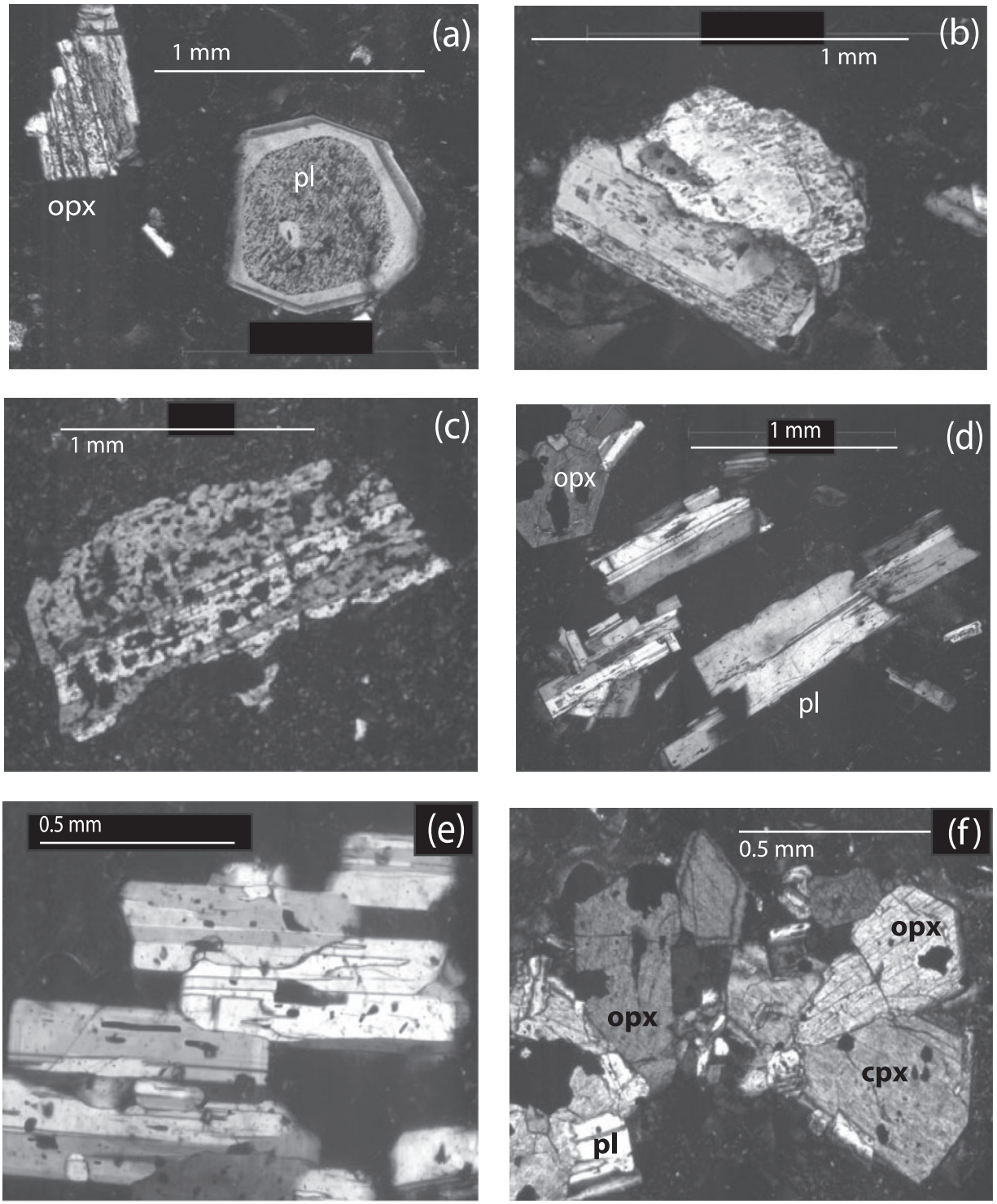

Fig. 3. Photomicrographs of plagioclase populations from the Cotopaxi andesites and rhyolites, showing (a) plagioclase with resorbed cores, (b) resorbed rims, (c) near entire resorption of plagioclase, (d) pristine crystals, (e) plagioclase crystals with melt inclusions and (f) an equilibrium intergrowth of plagioclase (pl), orthopyroxene (opx) and clinopyroxene (cpx) in one of the andesites. Scale bars are indicated.

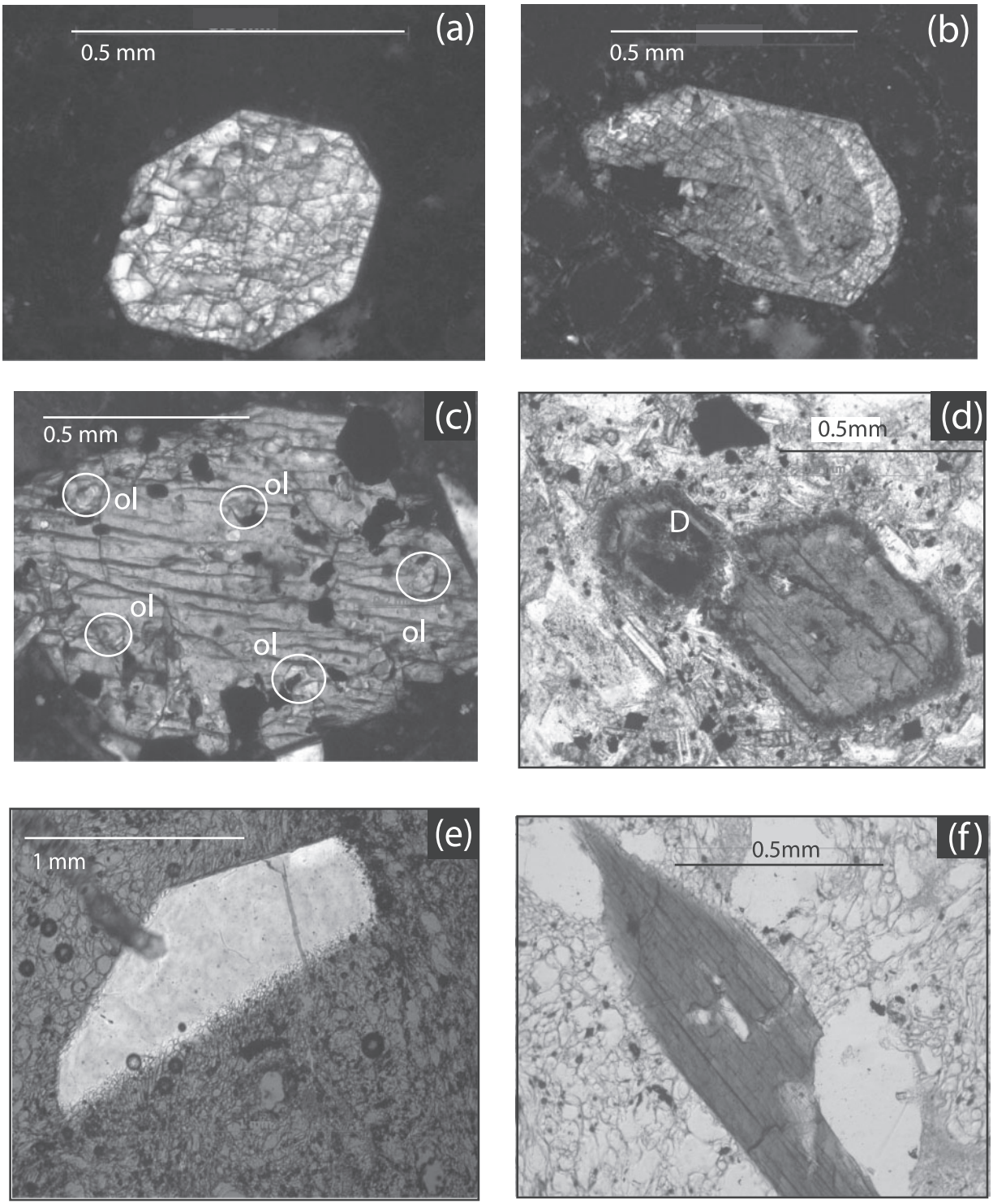

Fig. 4. Photomicrographs showing (a) a pristine orthopyroxene crystal in the Cotopaxi andesite, (b) a pristine clinopyroxene crystals with a Mg-rich core, (c) orthopyroxene with olivine inclusions in a basaltic andesite, (d) a highly resorbed amphibole in the Morurcu andesite, (e) pristine but broken plagioclase from the Cotopaxi rhyolite and (f) a pristine amphibole crystal in one of the Cotopaxi rhyolites. Scale bars are indicated.

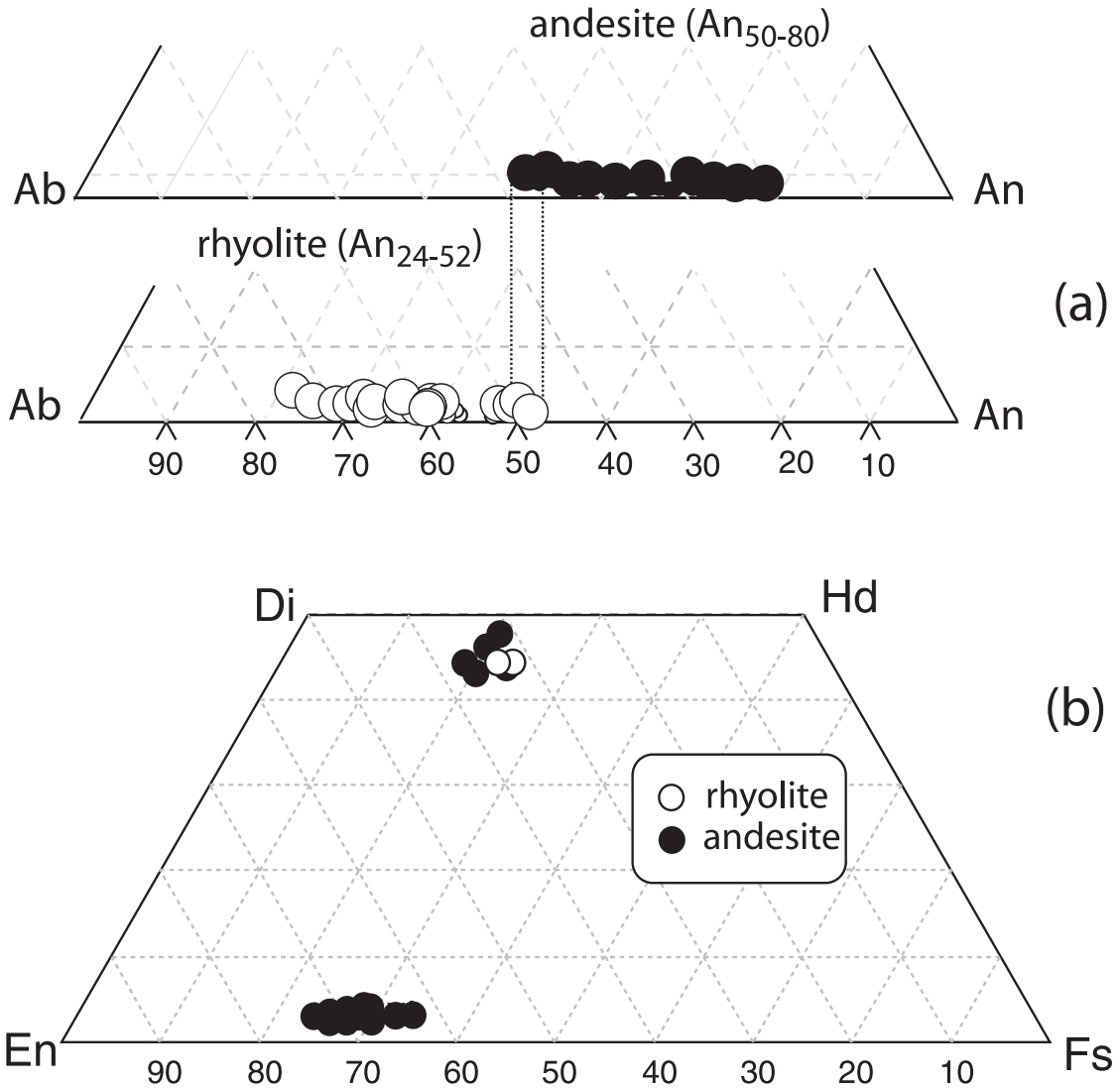

Fig. 5. (a) Anorthite content (An-number) in plagioclase from the Cotopaxi andesites ($An_{50–80}$) and rhyolites ($An_{24–52}$), showing slight overlap between the two compositions, as shown by the parallel dashed lines. (b) Pyroxene quadrilateral, showing the compositional range of the orthopyroxene and clinopyroxene in the rhyolites and andesites.

andesites (4–8) than in the rhyolites (12–16). The Ni concentrations range from 13–51 ppm in the basaltic andesites to 3–36 ppm in the andesites and 1–11 ppm in the rhyolites. The rhyolites are similar to the andesites, but are depleted with respect to P, Ti, MREE and HREE concentrations, and have higher concentrations of the LILE, LREE, Ta and Nb. Ta/Nb ratios in the rhyolites range from 0·08 to 0·1, compared with the andesites, which have constant Ta/Nb of 0·07. This observed variation correlates with a decrease in Sr concentrations between the andesites (480–695 ppm) and the rhyolites (220–320 ppm). The Chalupas rhyolites are shown for comparison with the Cotopaxi rhyolites in Fig. 7b. The Colorado Canyon is nearly identical in terms of trace elements to the Chalupas Caldera rhyolite.

Isotopes

Sr, Nd, and Pb isotopic compositions for the Cotopaxi samples and the Chalupas rhyolite are listed in Table 2. The Cotopaxi andesites and basaltic andesites have $^{87}Sr/^{86}Sr$ and $^{143}Nd/^{144}Nd$ that overlap with the rhyolite values (Fig. 8a inset). The average NVZ $^{87}Sr/^{86}Sr$ value of 0·70420 is only slightly higher than the Cotopaxi average of 0·70418. The Cotopaxi data are broadly similar to those for the accreted mafic terrane (Mamberti *et al.*, 2003) and volcanic rocks of the NVZ (Harmon *et al.*, 1984; Barragan *et al.*, 1998; Bryant *et al.*, 2006); they have lower $^{143}Nd/^{144}Nd$ than the Raspas Terrane (Bosch *et al.*, 2002) and mid-ocean ridge basalt (MORB). Cotopaxi $^{87}Sr/^{86}Sr$ values are slightly higher than MORB (White *et al.*, 1993).

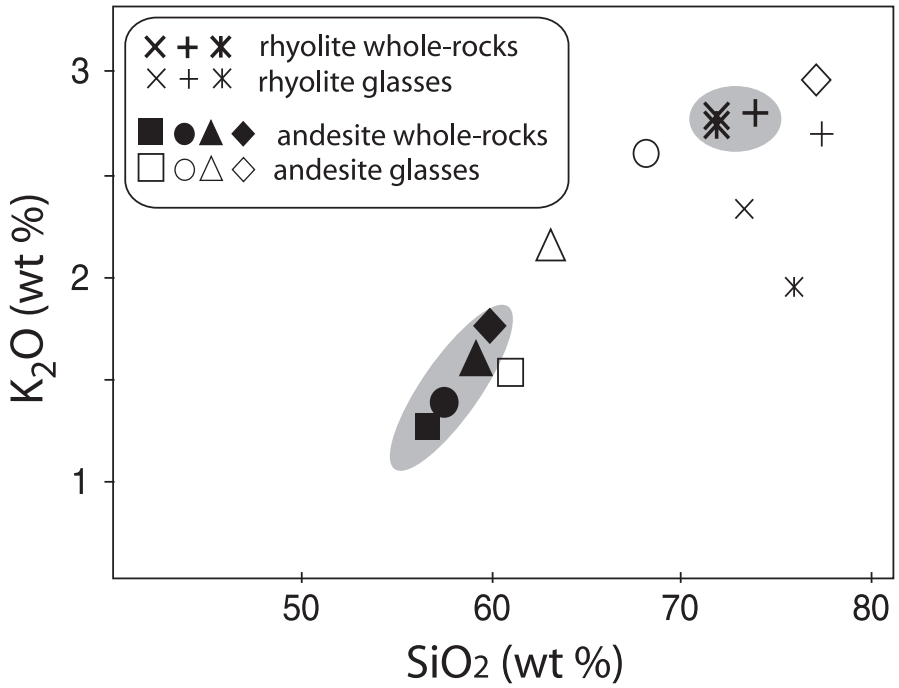

Fig. 6. K_2O vs SiO_2 for several glass and whole-rock pairs from Cotopaxi andesites and rhyolites. The whole-rock compositions are shown as shaded gray fields. Minerals were analyzed using the JEOL electron microprobe at UCLA. Data are given in Supplementary Data Table A1.

The Chalupas Caldera and Colorado Canyon samples have higher $^{87}Sr/^{86}Sr$ than the Cotopaxi samples.

The range in Pb isotope values for the Cotopaxi samples corresponds closely to the relatively narrow range of Pb isotope data from other NVZ volcanoes and accreted terrane reported by Harmon *et al.* (1984), Mamberti *et al.* (2003) and Chiaradia (2009) (Fig. 8b). Values for the Cotopaxi andesites overlap those of the rhyolites; the Colorado Canyon Ignimbrite has higher $^{207}Pb/^{204}Pb$ that is very similar to the Chalupas rhyolite. The greenschist-facies basement sample has lower $^{207}Pb/^{204}Pb$ and the same $^{206}Pb/^{204}Pb$ compared with the Cotopaxi andesites. Together, these data form a linear trend on a $^{207}Pb/^{204}Pb$ vs $^{206}Pb/^{204}Pb$ diagram that extends from Ecuadorian crust values (Raspas metapelite, Bosch *et al.*, 2002) to Nazca Plate MORB and Galapagos ocean island basalt (OIB) (Fig. 8b).

U-series isotopes (^{238}U–^{230}Th) were measured on mineral separates and whole-rocks from Cotopaxi, and have been previously published as part of a study to link the degree of U-series disequilibria in arc volcanic rocks to crustal thickness, a parameter that may exert some control over processes that fractionate U from Th (Garrison *et al.*, 2006). U-series data are typically represented as activity ratios that relate to the degree of equilibrium between (^{230}Th) and (^{238}U), and are also used to extract age information that relates to the time required for the system to return to equilibrium (Bourdon *et al.*, 2000; Hawkesworth *et al.*, 1997, 2000, 2004). Any activity ratio other than unity signifies fractionation of U from Th within the last 350 kyr. The ($^{238}U/^{230}Th$) for the Cotopaxi andesite whole-rocks ranges from 0·96 to 1·07 and the ($^{238}U/^{230}Th$) of the rhyolite whole-rocks ranges from 1·03 to 1·14 (i.e. 3–14% excess ^{238}U) (Fig. 9a). The ^{230}Th excesses in the andesites are attributed to mixing of arc magma with a 3–20% lower crustal eclogite melt, whereas the ^{238}U excesses in the Cotopaxi rhyolites are explained by fractionation of accessory allanite and apatite 74 kyr ago during rhyolite formation (Fig. 9c) (Garrison *et al.*, 2006). The overall conclusion from these data is that differentiation processes, rather than exclusively source processes, can control the partitioning of U and Th isotopes in continental arcs, and in evolved rocks, accessory phases such as allanite, apatite and zircon can create large ^{238}U or ^{230}Th excesses. A summary of this model is shown in Fig. 9c.

Whole-rock $\delta^{18}O$ values are listed in Table 3, and mineral–mineral equilibrium temperatures are shown in Appendix Fig. A4. Whole rock values vary from 6·42 to 8·27 (±0·42)‰ in the rhyolites and from 6·49 to 6·93 (±0·42)‰ in the andesites. The andesite glass has $\delta^{18}O$ values that are higher than the whole-rock values; however, on the basis of resorption and mixing textures, it is likely that some of the minerals are not in equilibrium with the glass in the andesites. Pristine textures of the minerals in the rhyolite indicate that they are probably in

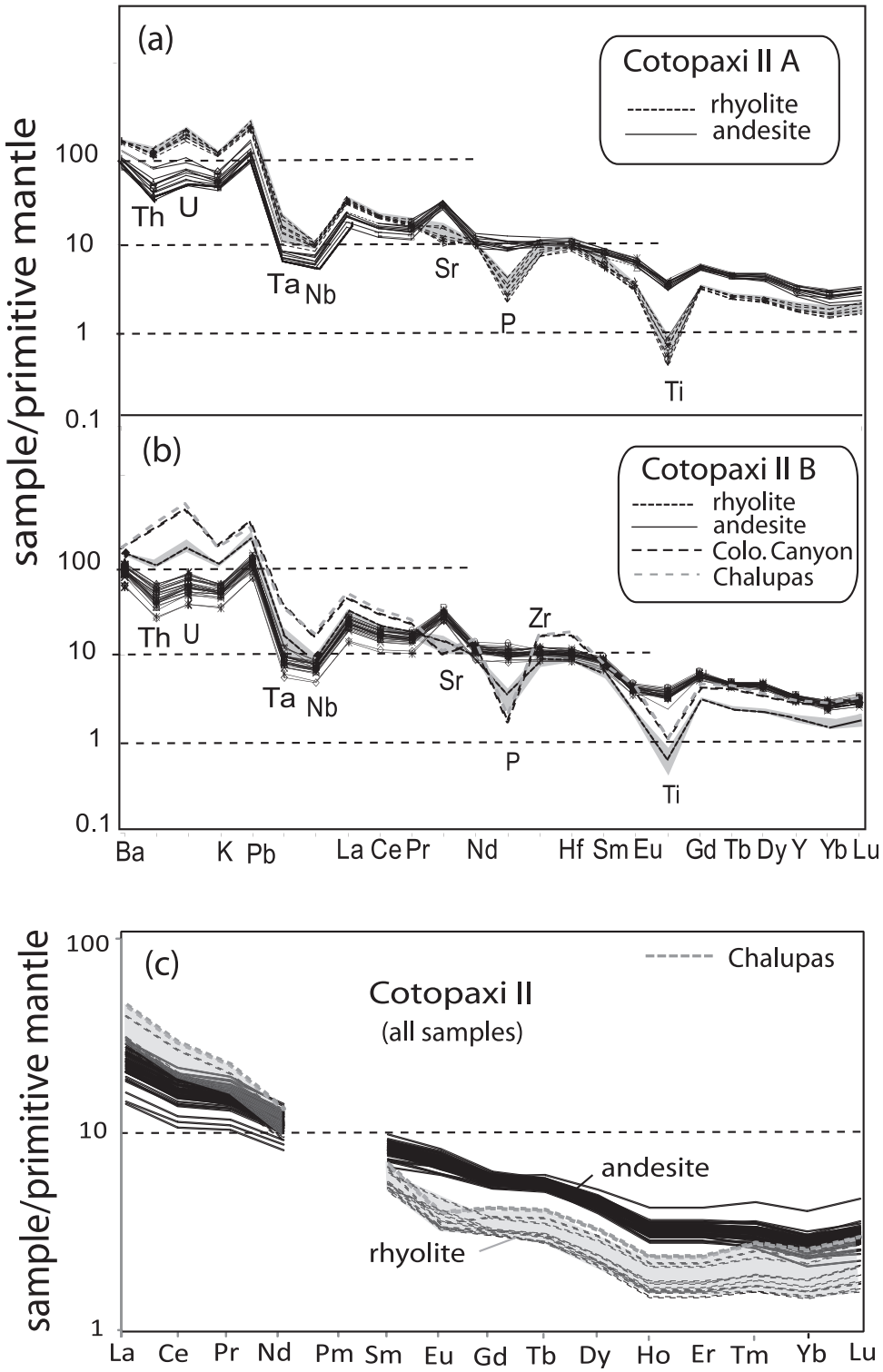

Fig. 7. Primitive mantle-normalized incompatible trace element diagrams for (a) the Cotopaxi IIA series and (b) Cotopaxi IIB series. The field for Cotopaxi rhyolite is shown for comparison (gray shaded). The Chalupas rhyolite is plotted for comparison with the Colorado Canyon rhyolite. Normalization factors from Sun & McDonough, (1989). (c) REE diagram for the rhyolites and andesites.

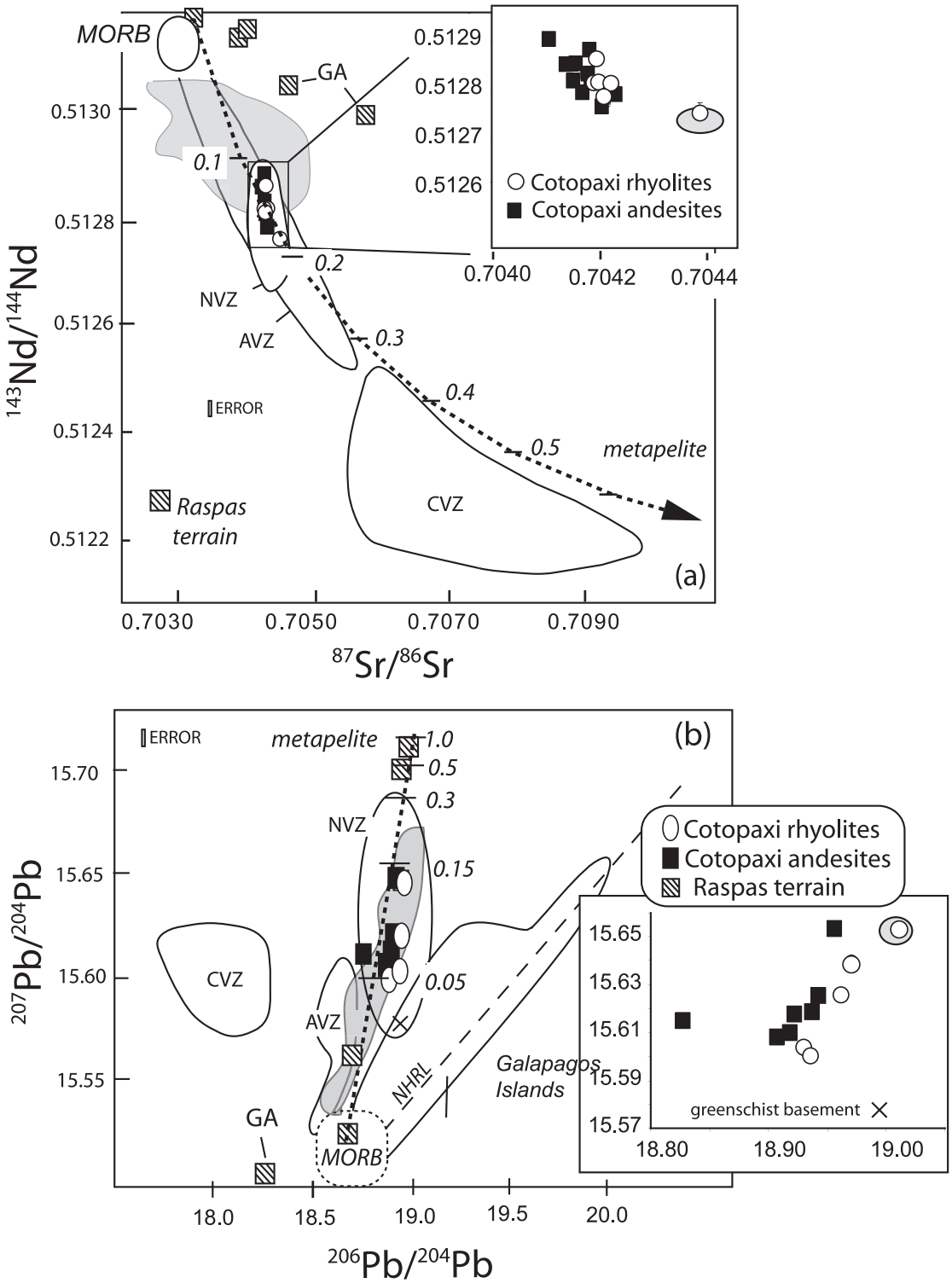

Fig. 8. (a) $^{87}Sr/^{86}Sr$ and $^{143}Nd/^{144}Nd$ isotopic variation for the volcanic rocks of the Andes of South America and for the Cotopaxi andesites and rhyolites (inset). Fields for the NVZ, AVZ and CVZ are from Bourdon *et al.* (2003). The gray shaded region is the field for accreted terrane data from the Macuchi Island Arc (Chiaradia, 2009) and Caribbean oceanic plateau (Mamberti *et al.*, 2003). GA, garnet amphibolite of the Raspas Terrane. Raspas Terrane data are from Bosch *et al.* (2002). Error bars are smaller than the symbols. Dashed line represents mixing between MORB and the Raspas metapelite ($^{87}Sr/^{86}Sr = 0{\cdot}722$, $^{143}Nd/^{144}Nd = 0{\cdot}512$). Numbers represent proportion of crust in the mix. The Cotopaxi data are consistent with a 10–20% contribution from the Raspas metapelite. (b) $^{206}Pb/^{204}Pb$ vs $^{207}Pb/^{204}Pb$ for the Cotopaxi rocks; fields for NVZ, AVZ and CVZ and the accreted terranes are the same as for (a). Cotopaxi data are shown in the inset. The Northern Hemisphere Reference Line (NHRL) is from Hart (1984). Dashed line represents mixing between MORB and Raspas metapelite. The Cotopaxi data are consistent with a 5–15% contribution from Raspas metapelite.

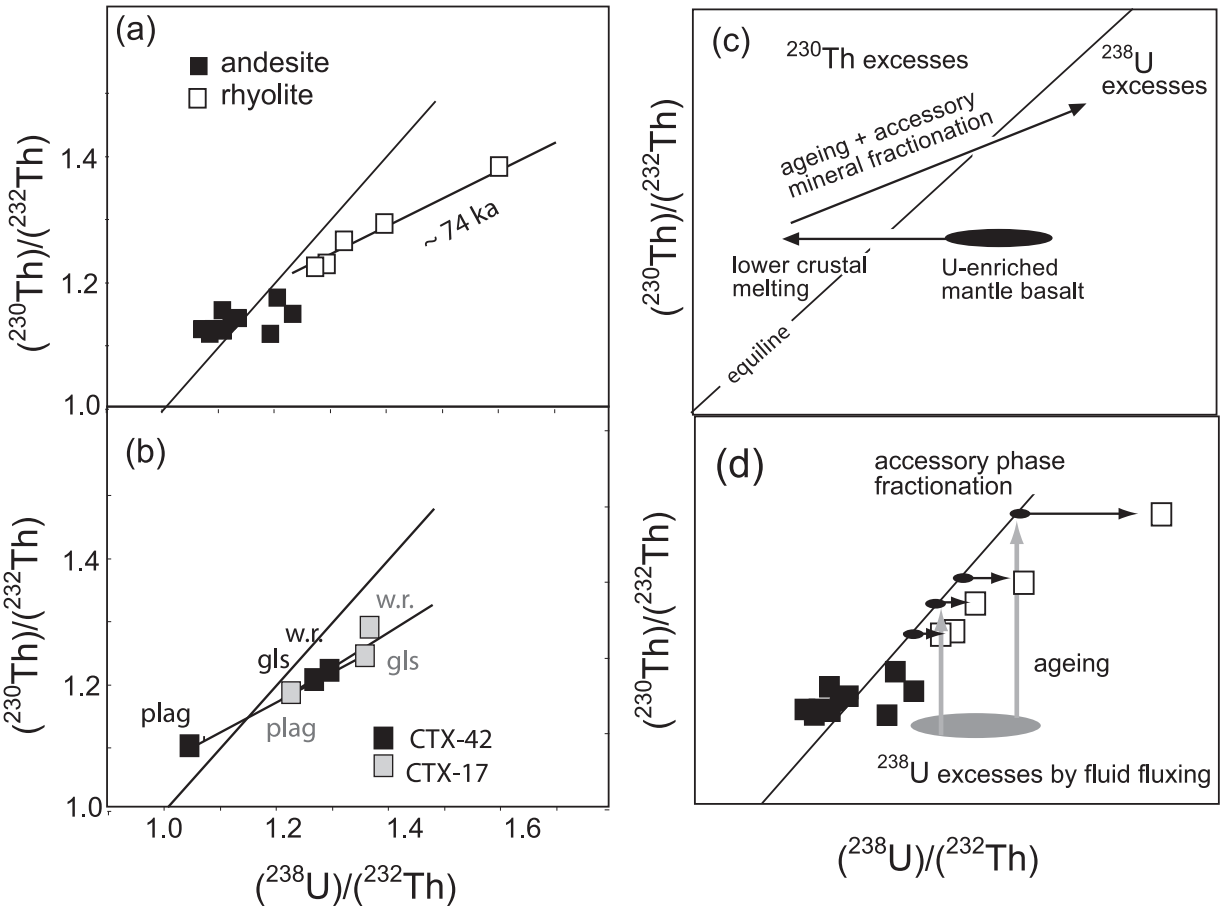

Fig. 9. (a) U-series data for Cotopaxi volcano andesites and rhyolites [for full discussion see Garrison *et al.* (2006)]. The andesite data span a range in $(^{238}U)/(^{230}Th)$ of 0·96–1·07, whereas the rhyolites have ^{238}U excesses of 3–14%. The linear array of rhyolite data points yields a U–Th age of 74 ka, inferred to be the crystallization time of the rhyolite reservoir. (b) Rhyolite mineral and glass separates and whole-rocks for two of the Cotopaxi rocks. (c) Generalized process diagram illustrating possible causes of U-series disequilibria, including ^{230}Th excesses through lower crustal melting, followed by ^{238}U excesses generated by accessory phase fractionation. (d) Alternative model to explain the U-series data. The grey shaded region represents hypothetical melts with ^{238}U excesses that cool and reach equilibrium, imparting a higher $(^{230}Th/^{232}Th)$ than the younger andesites. Re-melting of the older andesites followed by fractionation of accessory minerals produces rhyolites with ^{238}U excesses.

equilibrium and thus the rhyolite glass–mineral pairs give more realistic magmatic temperatures (Wolff *et al.*, 2002). Calculated glass–mineral $\delta^{18}O$ temperatures are in the range of 700–1400°C in the andesites and 470–900°C in the rhyolites (Fig. A4), and are correlated with SiO_2 content.

DISCUSSION

Source versus differentiation processes in the Cotopaxi andesites

In general, the sub-arc mantle source of arc magmas is thought to be imprinted with sediment and fluid signatures from the subducting oceanic lithosphere (Peacock, 1990; Turner *et al.*, 2000; Davidson *et al.*, 1991). The sediment signature is in part a function of eroded forearc crust (Plank & Langmuir, 1998), and in the NVZ this is likely to be of juvenile volcanogenic rocks from the accreted oceanic plateau (Mamberti, 2003) and/or the Macuchi island arc terrane (Chiaradia, 2009). The similarities in isotopic composition between these terranes, MORB and the Cotopaxi data, particularly with respect to $^{207}Pb/^{204}Pb$ (Fig. 8b), make it difficult to assess the effect of sediment subduction on the composition of the Cotopaxi lavas. However, a graph of $^{87}Sr/^{86}Sr$ vs $\delta^{18}O$ shows that crustal contamination is predominant over source contamination in this system (Fig. 10), and that the range in data can be explained by 5–20% contamination by radiogenic crust. The slab fluid signature, as identified by relative enrichments in the LILE, is clearly apparent in the Cotopaxi magmas, despite the lack of ^{238}U excesses in the andesites (Garrison *et al.*, 2006) that are typically associated with fluid addition (Turner *et al.*, 2000). One explanation for this is that the lower crustal melting process overprints

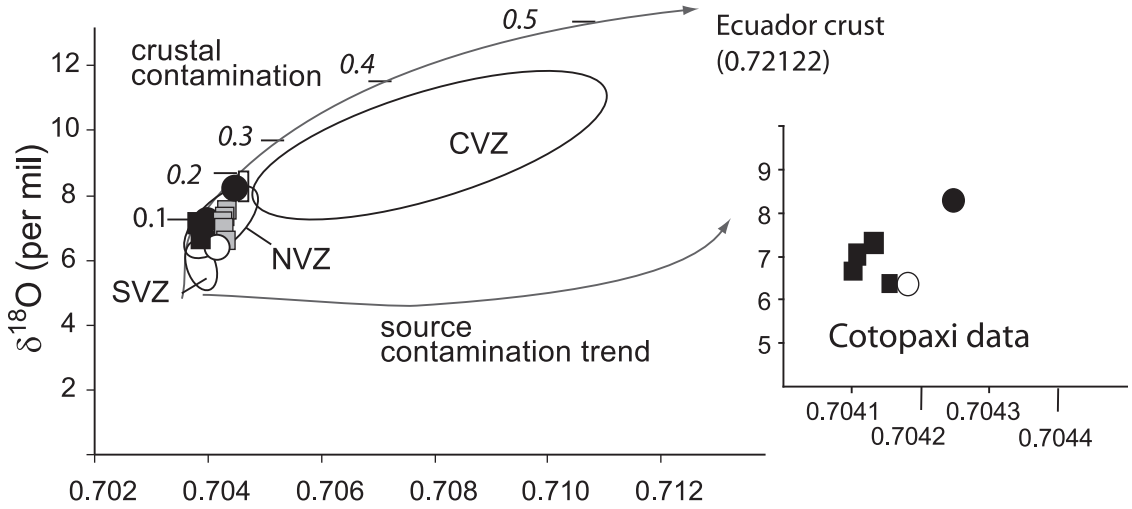

Fig. 10. $^{87}Sr/^{86}Sr$ vs $\delta^{18}O$ for the Cotopaxi whole-rocks and glasses, illustrating that the Cotopaxi data are consistent with a crustal assimilation rather than a source contamination trend. The crustal contamination trend was modeled using the same end-member as was used in Fig. 8 (i.e. the Raspas Terrane metapelite). The $\delta^{18}O$ value for this end-member was estimated on the basis of other radiogenic metapelitic rocks. Numbers represent the proportion of crust in the mix. The Cotopaxi data are consistent with 10–20% contamination by the Raspas metapelite, not the garnet amphibolite. Cotopaxi data from this study are shown in the inset. Fields for the Southern, Central and Northern Volcanic Zones are shown for comparison [data from Harmon *et al.* (1984) and James & Mucia, (1984)]. Error bars are smaller than the symbol sizes.

the fluid signature at Cotopaxi (Garrison *et al.*, 2006), a process also documented at Parinacota volcano in the CVZ (Hora *et al.*, 2009).

In terms of differentiation processes at Cotopaxi, the trace element data are consistent with lower crustal assimilation–fractional crystallization (AFC) processes, followed by magma mixing and mid- to upper crustal AFC. The Cotopaxi U-series data have been modeled previously using a 3–20% melt of garnet amphibolite as the assimilant by a primitive arc magma (Garrison *et al.*, 2006). However, a metapelitic schist is used as the lithology for lower crustal melting models in this study, for the reason that it provides a much better fit to the $^{87}Sr/^{86}Sr$ and $^{143}Nd/^{144}Nd$ isotope variation in the Cotopaxi data (Fig. 8). The AFC model illustrated in Fig. 11a (dashed line) shows the range of La/Yb and Sr values that are generated by a 7–15% partial melt of lower crust. Using a primitive basalt from Mt Shasta (Baker *et al.*, 1994) as a proxy for primitive arc basalt, we show that a mixture of arc basalt with lower crustal melts (shaded region in Fig. 11a) provides a reasonable fit to the Cotopaxi andesite data. The Sr–Nd–Pb isotope variation is also consistent with this model. The shift in the Cotopaxi data toward lower $^{143}Nd/^{144}Nd$ ratios is consistent with 10–20% assimilation of metapelitic crust (Fig. 8a). The $^{207}Pb/^{204}Pb$ compositions of the accreted NAB terrane span the entire range from MORB to Ecuadorian crust; however, the Cotopaxi data can be explained in terms of a 5–15% mixture between metapelite and MORB (Fig. 8b). In addition to consistently reproducing the isotope variation in the Cotopaxi rocks, the metapelitic schist is more likely to be the source of the Precambrian zircons in the Cotopaxi rocks than the mafic garnet amphibolite used by Garrison *et al.* (2006).

The role of crystal fractionation in the petrogenesis of the andesites was modeled using olivine, clinopyroxene, orthopyroxene, plagioclase and amphibole. Trace elements were modeled using the equations for fractional crystallization of Rollinson (1993), and the percentage of crystallization was compared with XLFRAC results (Table A2). Although amphibole is not observed in thin section, the La/Dy and Sr concentrations cannot be reproduced without amphibole in the crystallizing assemblage (Fig. 11b). Phase equilibria experiments show that amphibole is the dominant phase in andesitic liquids from 0·7 to 1·2 GPa (Alonso-Perez *et al.*, 2009), consistent with studies of amphibole-rich inclusions in arc lavas (e.g. Merapi, Chadwick *et al.*, 2010) and plutons (Larocque & Canil, 2009). A fractionating assemblage of amphibole (30%) + plagioclase (14%) + clinopyroxene (20%) + orthopyroxene (20%) + olivine (16%) reproduces the trend in the Cotopaxi andesites over a range of 10–50% crystallization ($F = 0{\cdot}9$–$0{\cdot}5$), consistent with XLFRAC calculations of 20–50%. The small amount of plagioclase crystallization is not uncommon in arcs and is believed to be caused by the high P_{H2O} of arc magmas, which causes suppression of plagioclase crystallization at lower crustal depths (Danyushevsky, 2001). Interestingly, the amphibole-bearing Morurcu andesites have Sr concentrations that decrease in tandem with La/Dy, consistent with the re-incorporation of MREE into the melt as amphibole becomes unstable at shallower depths. The highly resorbed texture of

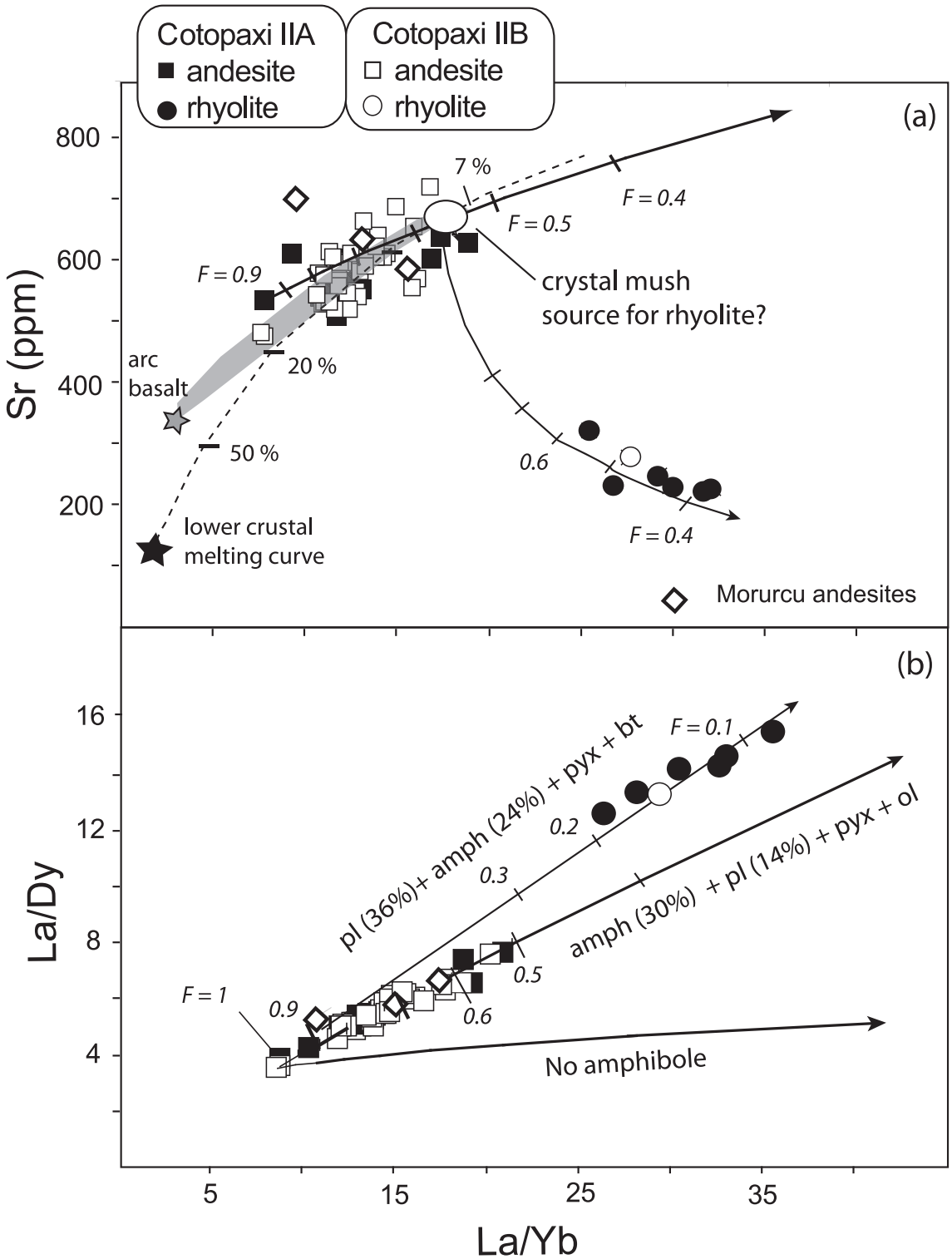

Fig. 11. (a) Sr (ppm) vs La/Yb, using the same crystallizing assemblage as in (b). The gray star represents the composition of arc basalt (Mt. Shasta, Baker *et al.*, 1994); the gray shaded region represents the range of mixtures of arc basalt with 7–15% partial melt of lower crust (black star). The melting model is illustrated by the black dashed line. The continuous black line represents crystallization of the same mineral assemblage from (b) for the andesite. The Morurcu vent samples are shown for comparison, and show a trend opposite of that to the younger andesites. *D* values used for models (Table A3) were experimentally derived for amphibole at 1000°C and 1·5 GPa (Brennan *et al.*, 1995). (b) La/Dy vs La/Yb, showing numerical models of fractional crystallization. *D* values are from Bacon & Druitt (1988) and Sisson & Bacon (1999). The andesites require crystallization of 30% amphibole + 14% plagioclase + pyroxene and olivine; the rhyolites could hypothetically be produced by crystallization of 36% plagioclase + 24% amphibole, plus biotite, quartz and accessory phases.

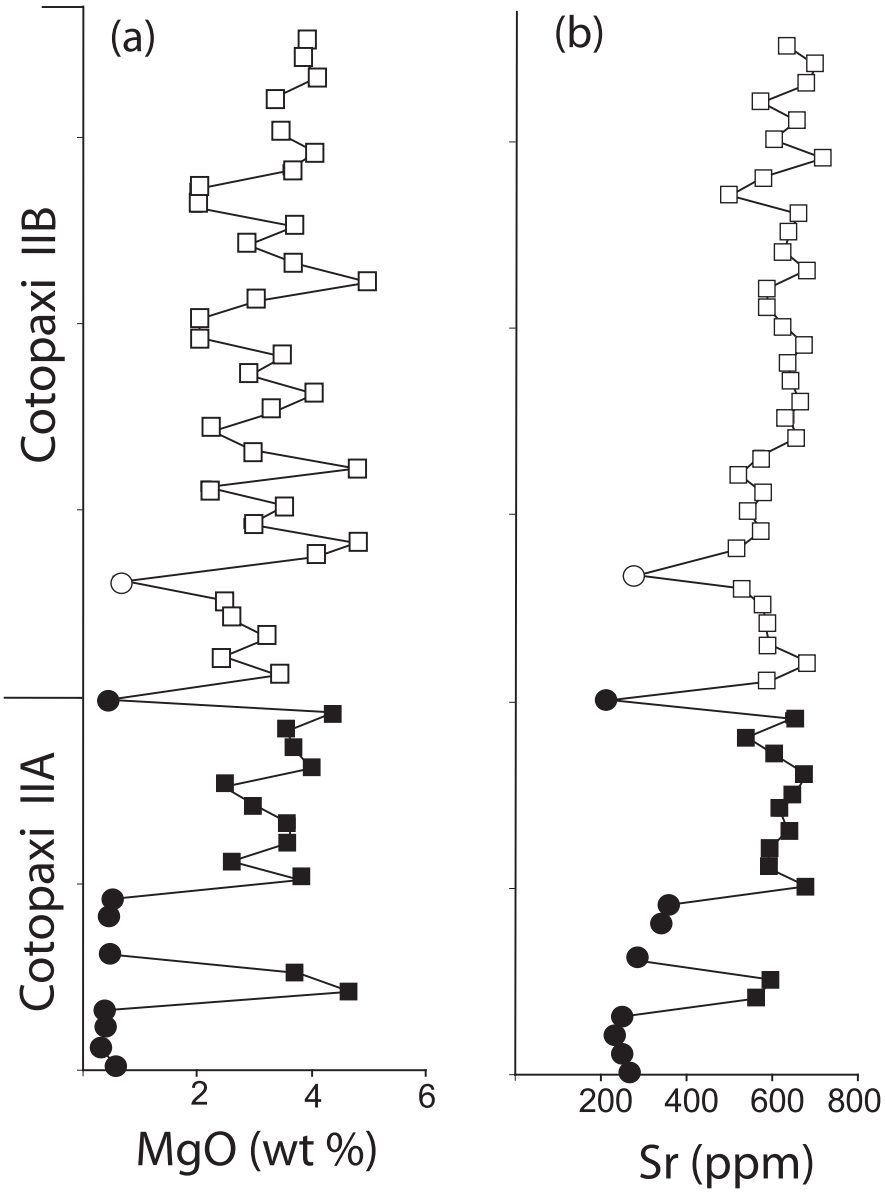

Fig. 12. Compositional and temporal variation in the Cotopaxi IIA and IIB sequences. Symbols are as in Fig. 2b and c. (a) Variation in wt % MgO over time for the Cotopaxi erupted rocks. (b) Variation in Sr content. These figures illustrate that (1) the system is frequently recharged, (2) the composition of the recharge magma is variable and (3) the system does not overall become progressively more evolved over time. Ages correspond to the generalized Cotopaxi II stratigraphy of Fig. 2a, younger than 13·2 ka.

the Morurcu amphibole crystals (Fig. 4d) indicates that amphibole was initially stable and dissolved during magma ascent (Davidson *et al.*, 2007; Ribeiro-Lauret, 2008).

Changes in pressure and temperature during magma ascent and storage are evident in the mineral textures. Inclusions of olivine in the basaltic andesite orthopyroxene (Fig. 4c) indicate that olivine was an early crystallizing phase, and pristine crystals of orthopyroxene and clinopyroxene in the andesites are consistent with the subsequent differentiation (Fig. 4a and b). Extensive resorption and zoning textures in the plagioclase crystals (Fig. 3a–d) record mixing of several batches of magma, a process that is common in most arc volcanoes (Davidson *et al.*, 1990; Volpe, 1992; Bourdon *et al.*, 2000; Cooper & Reid, 2003). Some of the crystals in the andesites (Fig. 3e and f) appear to be derived from disaggregated cumulates (Dungan & Davidson, 2004), also consistent with mixing and entrainment of crystals during magma ascent. Together with the stratigraphic variation, it appears that the magma reservoir at Cotopaxi volcano was recharged at least 16 times since 13·2 kyr ago (Fig. 12a and b).

Increases in the MgO and Sr contents of the erupted lavas indicate that the composition or alternatively the proportion of the recharge magma is variable, and the system has not become more evolved during the recent history of this volcano. There is no systematic general trend towards more (or less) evolved magmas through time among the andesites or the rhyolites, although the frequency of rhyolite eruptions is greater in the earlier eruptive phase studied in our work (Cotopaxi IIA).

The Cotopaxi rhyolites—small eruptions from a large reservoir?

The Cotopaxi rhyolites are somewhat enigmatic; even in continental arcs, repeated eruptions of rhyolite are uncommon at single arc volcanoes. In most cases, rhyolite is associated with large caldera systems where long storage times allow for extensive fractionation over time periods of 10^4–10^5 years (i.e. Yellowstone, Reid *et al.*, 1997; Toba, Vazquez & Reid, 2004; de Silva, 2008; Taupo, Charlier *et al.*, 2003), and dacites are increasingly believed to represent crystal-rich mush zones (Bachmann & Bergantz, 2004). Density and viscosity differences in the upper crust probably cause stalling of cooling magma (Feeley & Dungan, 1996; Thompson *et al.*, 2001), and one way that rhyolite is believed to form is by extraction of liquid from a reservoir of crystal mush [e.g. the 'rhyolite nursery' of Streck & Grunder (2007)]. The conditions most favorable for melt extraction have been calculated to be optimum between 50 and 70% crystallization (Dufek & Bachmann, 2010). In some systems, the crystal mush zone is reheated and mobilized by recharge (e.g. Fish Canyon dacite; Bachmann & Bergantz, 2003; Parat *et al.*, 2005).

Unlike large caldera eruptions (10^2–10^3 km^3), the Cotopaxi rhyolites are small volume (0·1–8 km^3), they were erupted in five events that are separated by as little as 2000 years, and they are erupted intermittently between andesite events. The U-series data yield a magma storage time of 74 kyr for these rhyolites (Garrison *et al.*, 2006; Fig. 9a). To reconcile this long timescale with the high frequency of rhyolite eruptions, however, requires that the reservoir is long-lived, but tapped at repeated intervals of several thousand years. Extraction of small batches of magma that erupt periodically, perhaps triggered by recharge (Watts *et al.*, 1999) or critical volume (0·1–8 km^3) and degassing, could explain the small-volume frequent eruptions and the aphyric texture of the rhyolites. We explain this by proposing that there is a long-lived mush zone, heated by fluxing andesite that contains a high-SiO_2 melt fraction that is periodically erupted. One problem with this model is the heat required to keep a large rhyolite reservoir thermally viable for 74 kyr, whilst producing only small increments of magma from the reservoir. If the rhyolite eruptions represent single batches of rhyolite liquid, then the U-series data require that there is a source with higher (^{230}Th/^{232}Th) that is melted or tapped to produce rhyolite eruptions. Remelting of old (>350 ka) andesites or dacites with high initial U excesses could explain this (Fig. 9d); however, it is difficult to explain the collinear mineral–glass isochrons for the Cotopaxi rhyolites (Fig. 9b).

Numerical models of gas-driven filter pressing (compaction) (McKenzie, 1984; Shirley, 1986; Philpotts *et al.*, 1996; Rabinowicz *et al.*, 2001) and hindered settling (Bachmann & Bergantz, 2004) were used to calculate how much time is required to physically separate the volumes of Cotopaxi rhyolite from a static crystal mush. We used estimated rhyolite volumes of 0·1–8·4 km^3 (Hall & Mothes, 2008) and the parameters and equations detailed by Bachmann & Bergantz (2004). A reservoir diameter of 7 km was used, on the basis of the diameter of the pre-existing Cotopaxi Caldera (Hall & Mothes, 2008). Melt-extraction models require that the interstitial glass in the crystal mush is rhyolitic, and that the crystals form an interlocking mesh (40–60% crystalline) (Bacon & Druitt, 1988; Sisson & Bacon, 1999; Hildreth & Fierstein, 2000). The Cotopaxi andesite glass compositions range from 60 to 78 wt% SiO_2 (Fig. 4). Figure 11b shows that the rhyolites could reasonably be derived from an andesite that is within the range of 40–50% crystalline. To generate the ~8 km^3 of the largest Cotopaxi rhyolite using hindered settling requires 2000 years; compaction, on the other hand requires 45 kyr to produce the same volume of magma. These models show that to generate the smallest erupted volume (0·1 km^3) using the hindered settling model requires ~300 years, but using compaction requires 2000 years. On the basis of these models, timescales of rhyolite formation (10^5 years for 8·4 km^3) are roughly consistent with the U-series estimates of 74 kyr; the small volume eruption estimates are consistent with the 2000 year repose interval of the Cotopaxi rhyolites. If the Cotopaxi U-series data represent a protracted crustal storage time (~74 kyr), then small melt fractions removed from the crystal mush must represent aliquots removed as the entire system ages. Alternatively, if the rhyolites represent small batches of magma, formed over ~300–2000 years, then each batch must represent melting or remobilization of andesite or dacite mush that has aged for sufficient time (>350 kyr) that it is close to equilibrium and therefore has higher (^{230}Th/^{232}Th) than the most recent andesites. Extraction of rhyolite from a dacitic mush has been suggested to be an important process in the formation of continental crust [i.e. the 'quantum magmatism' model of Dufek & Bachmann (2011)]. Accessory mineral fractionation (apatite, allanite, monzanite) from the rhyolite liquid creates the observed ^{238}U excesses (Fig. 9d). The rhyolite mineral isochrons are not explained by this model, and require further analysis.

The geochemical evidence that supports rhyolite formation by melt extraction from an andesite crystal mush

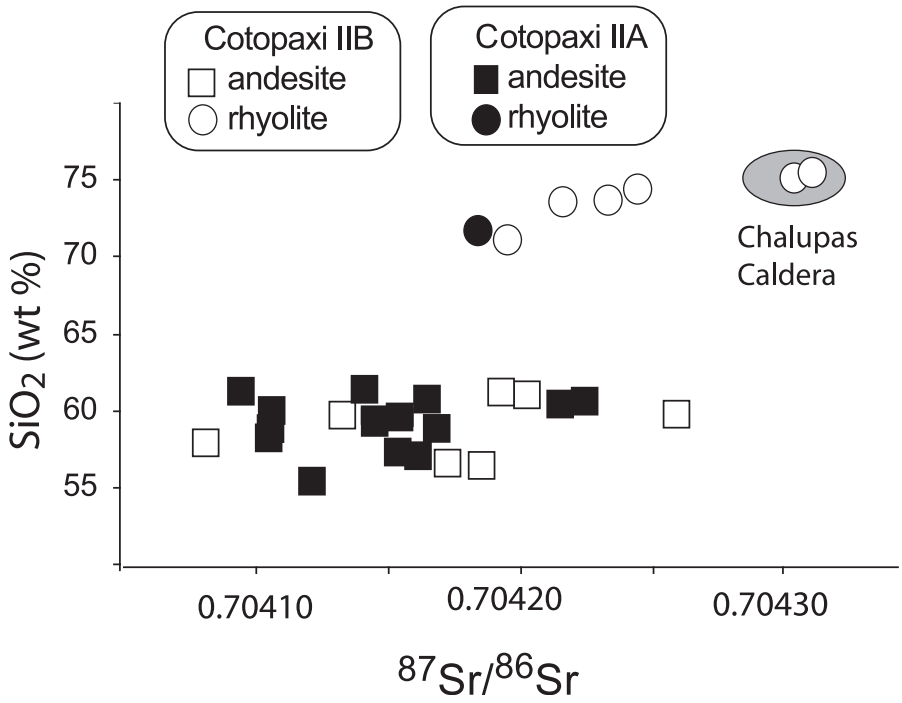

Fig. 13. $^{87}Sr/^{86}Sr$ vs wt % SiO_2 for the Cotopaxi rocks, illustrating that there is no correlation between differentiation and $^{87}Sr/^{86}Sr$, as might be expected if differentiation is related to crustal contamination. Colorado Canyon samples plot within the region of Chalupas ignimbrite compositions. Errors are smaller than the symbol size.

includes the overlapping $^{87}Sr/^{86}Sr$ and $^{143}Nd/^{144}Nd$ isotope compositions of the rhyolites and andesites (Fig. 8). Also, the compositions of the plagioclase crystals from the rhyolitic magma ($An_{24–50}$; Fig. 4) do not overlap with the composition of the andesite plagioclase ($An_{50–80}$), which, in addition to the pristine texture of the rhyolite plagioclase, suggests that the crystals formed in a separate, more evolved magma reservoir. The clinopyroxene crystals in one of the rhyolites have the same composition as the andesite clinopyroxene (Fig. 4b), which suggests that these crystals formed in an andesitic magma and were entrained during segregation of the rhyolite from the andesite matrix. Physical evidence for crustal assimilation in the Cotopaxi system is the recycled Precambrian zircon crystals that are found in the rhyolite (Appendix Fig. A3). It is impossible to know at what point the zircons were inherited by the magma, although the lack of correlation between $^{87}Sr/^{86}Sr$ and wt % SiO_2 (Fig. 13) suggests that is not related to rhyolite formation by melting of radiogenic upper crust, which would have imparted a higher $^{87}Sr/^{86}Sr$ signature to the rhyolite (Hildreth and Moorbath, 1988). We propose that the rhyolites formed by segregation of melt with 62–78 wt % SiO_2 (Fig. 4) from an andesite mush containing clinopyroxene, orthopyroxene and plagioclase. Crystallization of plagioclase (50%) + amphibole (25%) + biotite (15%) + quartz (8%) + accessory minerals (2%) produced the Cotopaxi rhyolites over a range of 40–60% crystallization, consistent with the observed trace element variation (Fig. 11). The Colorado Canyon rhyolite is an exception to the proposed model, as it does not fit geochemically with the Cotopaxi rhyolites, but is very similar to the Chalupas rhyolite, despite having a documented age of 4500 years. If it is related to the Chalupas system, then it may represent part of the Chalupas rhyolite that was remobilized and erupted, although how this fits into the model for melt extraction is unclear.

SUMMARY AND CONCLUSIONS

(1) The petrogenetic processes that formed the Cotopaxi andesites include assimilation of lower crustal melts of crust similar to the metapelitic schist of the Raspas Terrane (Fig. 14, box 1). Lower crustal melts (5–20%) of metapelitic crust mix with primitive basalt, creating the range, albeit limited, in $^{143}Nd/^{144}Nd$, $^{87}Sr/^{86}Sr$ and $^{207}Pb/^{204}Pb$ that is observed in the Cotopaxi rocks. This contamination model is also consistent with the oxygen isotope compositions of the Cotopaxi rocks and previously published U-series data (Garrison *et al.*, 2006). Andesite magma ascending from the lower crust entrains intergrowths of disaggregated crystal mush; crystals of amphibole that were stable in the lower crust dissolve during ascent.

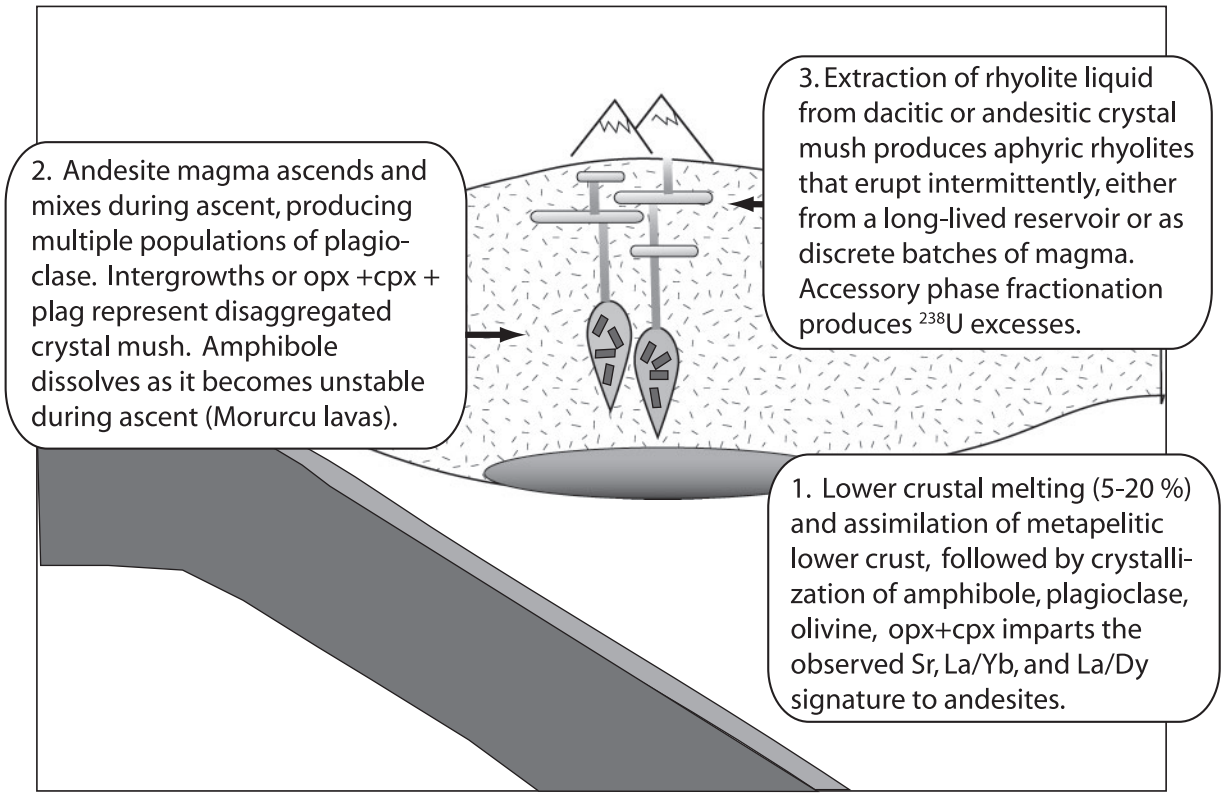

Fig. 14. Schematic petrogenetic model used to explain the geochemical variation among the Cotopaxi andesites and rhyolites [modified from Garrison *et al.* (2006)]. Boxes described in text.

(2) Minerals from the Cotopaxi rhyolites and andesites record a rich petrogenetic history, including early crystallization of olivine, followed by fractionation of clinopyroxene + orthopyroxene + plagioclase. Amphibole, although not a stable phase during eruption, is an important phase in the early stages of magma genesis; the observed trace element variation cannot be reproduced in the absence of hornblende crystallization. Extensive mixing is recorded by at least four populations of plagioclase crystals, and the stratigraphy records at least 16 magma recharge events in the past 13·2 kyr (Fig. 14, box 2). Rising magma batches are shown as diapirs from the lower crust (not to scale) in Fig. 14; however, magma transfer in the upper crust is more likely to take place via fractures and dikes (Vigneresse & Clemens, 2000).

(3) The Cotopaxi rhyolites were formed in the upper crust by melt extraction from an andesitic or dacitic crystal mush ~74 kyr ago, followed by crystallization of plagioclase, amphibole and biotite (Fig. 14, box 3). Small batches of rhyolite magma were periodically erupted from a large magma reservoir, perhaps triggered by reheating by andesite (or dacite) magma. Alternatively, the rhyolite eruptions could represent remelting of a crystal mush that had an initial ^{238}U excess and was older than 350 ka. Zircon crystals in the rhyolites record assimilation of the 2·1 Ga crust of the South American craton.

The configuration of the rhyolite–andesite plumbing system at Cotopaxi is not clear from the results of this study. What controls the eruption of the rhyolite batches, particularly in the midst of repeated andesite eruptions? How does this relate to the timescales suggested by the existing U-series data? These questions remain to be answered, particularly regarding the short repose time and small volumes of the rhyolite eruptions and the trigger for andesite vs rhyolite eruptions. Nevertheless, we have shown that combining stratigraphy with geochemistry adds a valuable component to studies of arc volcanoes and the evolution of continental arcs over time. These data reveal the many intricate processes involved in the sub-volcanic plumbing system of arc volcanoes that ultimately contribute to the formation of continental crust.

ACKNOWLEDGEMENTS

This paper has greatly benefited by thoughtful and thorough reviews by Gene Yogodzinsky, Dennis Geist and an

anonymous reviewer. We also thank Mary Reid, Frank Ramos, Frank Tepley, John Hora and fellow students and staff at UCLA for helpful discussions during the development of this project. We also thank Dave Mattey and Dave Lowry at Royal Holloway, University of London for their help with oxygen isotope analyses, and the students (Indira Molina and Alex Garcia) at the IGEPN in Quito, Ecuador for their help with field support.

FUNDING

Funding for this research was provided by the National Science Foundation (NSF), grant #EAR 9980407. Garrison also received a Geological Society of America student research grant and funding from the UCLA Latin American Studies program.

SUPPLEMENTARY DATA

Supplementary data for this paper are available at *Journal of Petrology* online.

REFERENCES

Alonso-Perez, R., Müntener, O. & Ulmer, P. (2009). Igneous garnet and amphibole fractionation in the roots of island arcs: experimental constraints on andesitic liquids. *Contributions to Mineralogy and Petrology* **157**, 541–558.

Arculus, R. J., Lapierre, H. & Jaillard, E. (1999). Geochemical window into subduction and accretion processes: Raspas Metamorphic Complex, Ecuador. *Geology* **27**, 547–550.

Bachmann, O. & Bergantz, G. W. (2003). Rejuvenation of the Fish Canyon magma body: a window into the evolution of large-volume silicic magma systems. *Geology* **31**, 789–792.

Bachmann, O. & Bergantz, G. W. (2004). On the origin of crystal-poor rhyolites: extracted from batholithic crystal mushes. *Journal of Petrology* **45**, 1565–1582.

Bacon, C. R. & Druitt, T. H. (1988). Compositional evolution of the zoned calcalkaline magma chamber of Mount Mazama, Crater Lake, Oregon. *Contributions to Mineralogy and Petrology* **98**, 224–256.

Baker, M. B., Grove, T. L. & Price, R. (1994). Primitive basalts and andesites from the Mt. Shasta region, N. California: products of varying melt fraction and water content. *Contributions to Mineralogy and Petrology* **118**, 111–129.

Barberi, F., Coltelli, M., Frullani, A., Rosi, M. & Almeida, E. (1995). Chronology and dispersal characteristics of recently (last 5000 years) erupted tephra of Cotopaxi (Ecuador): implications for long term eruptive forecasting. *Journal of Volcanology and Geothermal Research* **69**, 217–239.

Barragan, R., Geist, D., Hall, M., Larson, P. & Kurz, M. (1998). Subduction controls on the compositions of lavas from the Ecuadorian Andes. *Earth and Planetary Science Letters* **154**, 153–166.

Bigazzi, G., Coltelli, M., Hadler, J. & Osorio, A. (1997). Provenance studies of obsidian artifacts using fission track analyses in South America: An overview. In: Daniel, B. Verniers (ed.) . *in Noticias de Antropología y Arqueología Mem. 49th Cong. Intern. Americanistas, Quito, ARQ* **14**, 1–16.

Bosch, D., Gabriele, P., Lapierre, H., Malfere, J.-L. & Jaillard, E. (2002). Geodynamic significance of the Raspas Metamorphic Complex (SW Ecuador): geochemical and isotopic constraints. *Tectonophysics* **345**, 83–102.

Bottinga, Y. & Javoy, M. (2000). Oxygen isotope partitioning among the minerals in igneous and metamorphic rocks. *Reviews of Geophysics and Space Physics* **13**, 401–418.

Bourdon, B., Worner, G. & Zindler, A. (2000). U-series evidence for crustal involvement and magma residence times in the petrogenesis of Parinacota volcano, Chile. *Contributions to Mineralogy and Petrology* **139**, 458–469.

Bourdon, E., Eissen, J-P., Gutscher, M-A., Monzier, M., Hall, M. & Cotton, M. (2003). Magmatic response to early aseismic ridge subduction: the Ecuadorian margin case (South American). *Earth and Planetary Sciences Letters* **205**, 123–138.

Brenan, J. M., Shaw, H. F., Ryerson, F. J. & Phinney, D. L. (1995). Experimental determination of trace element partitioning between pargasite and a synthetic hydrous andesitic melt. *Earth and Planetary Science Letters* **135**, 1–11.

Bryant, J. A., Yogodzinski, G. M., Hall, M. L., Lewicki, J. L. & Bailey, D. G. (2006). Geochemical constraints on the origin of volcanic rocks from the Andean Northern Volcanic Zone, Ecuador. *Journal of Petrology* **47**, 1147–1175.

Chadwick, J. P., Troll, V. R., Schulz, B., Dallai, L., Freda, C., Schwarzkopf, L. M., Annersten, H. & Skogby, H. (2010). The role of amphibole in Merapi arc magma petrogenesis: insights from petrology and geochemistry of lava hosted xenoliths and xenocrysts. *EGU General Assembly* 15379.

Charlier, B. L. A., Peate, D. W., Wilson, C. J. N., Lowenstern, J. B., Storey, M. & Brown, S. J. A. (2003). Crystallization ages in coeval silicic magma bodies: ^{238}U–^{230}Th disequilibrium evidence from the Rotoiti and Earthquake Flat eruption deposits, Taupo Volcanic Zone, New Zealand. *Earth and Planetary Science Letters* **206**, 441–457.

Chiaradia, M. (2009). Adakite-like magmas from fractional crystallization and melting–assimilation of mafic lower crust (Eocene Macuchi arc, Western Cordillera, Ecuador). *Chemical Geology* **265**, 468–487.

Chiba, H., Chacko, T., Clayton, R. N. & Goldsmith, J. R. (1989). Oxygen isotope fractionations involving diopside, forsterite, magnetite and calcite: Application to thermometry. *Geochimica et Cosmochimica Acta* **53**, 2985–2995.

Cooper, K. M. & Reid, M. R. (2003). Re-examination of crystal ages in recent Mount St. Helens lavas: implications for magma reservoir processes. *Earth and Planetary Science Letters* **213**, 149–167.

Dalrymple, B. G., Grove, M., Lovera, O. M., Harrison, T. M., Hulen, J. B. & Lanphere, M. A. (1999). Age and thermal history of the Geysers plutonic complex (felsite unit), Geysers geothermal field, California: a $^{40}Ar/^{39}Ar$ and U–Pb study. *Earth and Planetary Science Letters* **173**, 285–298.

Danyushevsky, L. V. (2001). The effect of small amounts of H_2O on crystallization of mid-ocean ridge and backarc basin magmas. *Journal of Volcanology and Geothermal Research* **110**, 265–280.

Davidson, J. P. (1996). Deciphering mantle and crustal signatures in subduction zone magmatism. In: Bebout, Gray, E., Scholl, D. W., Kirby, S. H. & Platt, J. P. (eds) *Subduction, Top to Bottom. Geophysical Monograph, American Geophysical Union* **96**, 251–261.

Davidson, J. P., McMillan, N. J., Moorbath, S., Worner, G., Harmon, R. S. & Lopez-Escobar, L. (1990). The Nevados de Payachata volcanic region (18°S, 69°W, N. Chile) II. Evidence for widespread crustal involvement in Andean magmatism. *Contributions to Mineralogy and Petrology* **105**, 412–432.

Davidson, J. P., Harmon, R. S. & Worner, G. (1991). The source of central Andean magmas; some considerations. *Geological Society of America, Special Papers* **265**, 233–243.

Davidson, J. P., Turner, S. P., Handley, H., Macpherson, C. & Dosseto, A. (2007). Amphibole 'sponge' in arc crust? *Geology* **35**, 787–790.

de Silva, S. (2008). Arc magmatism, calderas, and supervolcanoes. *Geology* **36**, 671–672.

Dungan, M. A. & Davidson, J. P. (2004). Partial assimilative recycling of the mafic plutonic roots of arc volcanoes: An example from the Chilean Andes. *Geology* **32**, 773–776.

Dufek, J. & Bachman, O. (2010). Quantum magmatism: Magmatic compositional gaps generated by melt-crystal dynamics. *Geology* **38**, 687–690.

Feeley, T. C. & Dungan, M. A. (1996). Compositional and dynamic controls on mafic–silicic magma interactions at continental arc volcanoes: evidence from Cordon El Guadal, Tatara–San Pablo Complex, Chile. *Journal of Petrology* **37**, 1547–1577.

Feininger, T. (1980). Eclogite and related high-pressure regional metamorphic rocks from the Andes of Ecuador. *Journal of Petrology* **21**, 107–140.

Feininger, T. & Se guin, M. K. (1983). Simple Bouguer gravity anomaly field and the inferred crustal structure of continental Ecuador. *Geology* **11**, 40–44.

Garrison, J. M. (2004). Timescales of petrogenetic processes at Cotopaxi volcano, Northern Volcanic Zone, Ecuador, PhD dissertation, UCLA, Los Angeles, CA, 417 pp.

Garrison, J. M., Davidson, J. P., Reid, M. & Turner, S. P. (2006). Source versus differentiation controls on U-series disequilibria: Insights from Cotopaxi Volcano, Ecuador. *Earth and Planetary Science Letters* **4**, 548–565.

Guillier, B., Chatelain, J. L., Jaillard, E., Poupinet, G. & Fels, J. F. (2001). Seismological evidence on the geometry of the orogenic system in central–northern Ecuador (South America). *Geophysical Research Letters* **28**, 3749–3752.

Hall, M. & Mothes, P. (2008). The rhyolitic–andesitic eruptive history of Cotopaxi volcano, Ecuador. *Bulletin of Volcanology* **70**, 675–702.

Hall, M. & von Hillebrandt, C. (1988). Mapa de los peligrosas volcánicos potenciales asociados con el volcán Cotopaxi: 1) zona norte y 2)zona sur. Quito: Instituto Geofisico.

Hammersley, L., DePaolo, D. J. & Beate, B. Chalupas Caldera, Ecuador: A study of the development of a large volume rhyolite system in the northern Andes. IAVCEI General Assembly.

Harmon, R. S., Barreiro, B. A., Moorbath, S., Hoefs, J., Francis, P. W., Thorpe, R. S., Deruelle, B., McHugh, J. & Viglino, J. A. (1984). Reginal O-, Sr-, and Pb-isotope relationships in late Cenozoic calc-alkaline lavas of the Andean Cordillera. *Journal of the Geological Society, London* **141**, 803–822.

Hart, S. R. (1984). A large-scale isotope anomaly in the Southern Hemisphere mantle. *Nature* **309**, 753–757.

Hawkesworth, C. J., Turner, S. P., McDermott, F., Peate, D. W. & van Calsteren, P. (1997). U–Th isotopes in arc magmas: implications for element transfer from the subducted crust. *Science* **276**, 551–555.

Hawkesworth, C. J., Blake, S., Evans, P., Hughes, R., Macdonald, R., Thomas, L. E., Turner, S. P. & Zellmer, G. (2000). Time scales of crystal fractionation in magma chambers—integrating physical, isotopic and geochemical perspectives. *Journal of Petrology* **41**, 991–1006.

Hawkesworth, C., George, R., Turner, S. & Zellmer, G. (2004). Time scales of magmatic processes. *Earth and Planetary Science Letters* **218**, 1–16.

Hildreth, W. & Fierstein, J. (2000). Katmai volcanic cluster and the great eruption of 1912. *GSA Bulletin* **112**, 1594–1620.

Hildreth, W. & Moorbath, S. (1988). Crustal contributions to arc magmatism in the Andes of central Chile. *Contributions to Mineralogy and Petrology* **98**, 455–489.

Hora, J. M., Singer, B. S., Worner, G., Beard, B., Jicha, B. R. & Johnson, C. M. (2009). Shallow and deep crustal control on differentiation of calc-alkaline and tholeiitic magma. *Earth and Planetary Science Letters* **285**, 75–86.

Hughes, R. A. & Pilatasig, L. F. (2002). Cretaceous and Tertiary terrain accretion in the Cordillera Occidental of the Andes of Ecuador. *Tectonophysics* **345**, 29–48.

James, D. E. & Murcia, A. L. (1984). Crustal contamination in northern Andean volcanics. *Journal of the Geological Society, London* **141**, 823–830.

Johnson, D. M., Hooper, P. R. & Conrey, R. M. (1999). XRF analysis of rocks and minerals for major and trace elements on a single low dilution Li-tetraborate fused bead. *Advances in X-ray Analysis* **41**, 843–867.

Knaak, C., Cornelius, S. B. & Hooper, P. R. (1994). *Technical Notes: Trace Element Analyses of Rocks and Minerals by ICP-MS*. Pullman, WA: GeoAnalytical Lab, Washington State University.

Larocque, J. & Canil, D. (2009). The role of amphibole in the evolution of arc magmas and crust: the case from the Jurassic Bonanza arc section, Vancouver Island, Canada. *Contributions to Mineralogy and Petrology* **159**, 475–492.

Le Maitre, R. W., Bateman, P., Dudek, A., Keller, J., Lameyre, J., Le Bas, M. J., Sabine, P. A., Schmid, R., Sorenson, H., Streckeisen, A., Woolley, A. R. & Zanettin, B. (1989). *A Classification of Igneous Rocks and a Glossary of Terms*. Oxford: Blackwell, 342 p.

Lonsdale, P. (1978). Ecuadorian subduction system. *AAPG Bulletin* **62**, 2454–2477.

Mamberti, M., Lapierre, H., Bosch, D., Jaillard, E., Ethien, R., Hernandez, J. & Polvé, M. (2005). Accreted fragments of the Late Cretaceous Caribbean–Colombian Plateau in Ecuador. *Lithos* **66**, 173–199.

McCourt, W. J., Aspden, J. A. & Brook, M. (1984). New geological and geochronological data from the Colombian Andes: continental growth by multiple accretion. *Journal of the Geological Society, London* **141**, 831–845.

McKenzie, D. (1984). The generation and compaction of partially molten rock. *Journal of Petrology* **25**, 713–765.

Mothes, P. (1992). Lahars of Cotopaxi volcano, Ecuador: hazard and risk evaluation. In: McCall, G. J. H., Laming, D. J. C. & Scott, S. C. (eds) *Geohazards, Natural and Man-made*. London: Chapman and Hall, pp. 53–64.

Mothes, P., Hall, M. & Janda, R. (1998). The enormous Chillos valley lahar: an ash-flow generated debris flow from Cotopaxi volcano, Ecuador. *Bulletin of Volcanology* **59**, 233–244.

Mothes, P., Hall, M., Andrade, D., Samaniego, P., Pierson, T., Ruiz, G. & Yepes, H. (2004). Character, stratigraphy and magnitude of historical lahars of Cotopaxi volcano, Ecuador. *Acta Volcanologica* **16**, 85–107.

Parat, F., Dungan, M. A. & Lipman, P. W. (2005). Contemporaneous trachyandesitic and calc-alkaline volcanism of the Huerto Andesite, San Juan Volcanic Field, Colorado, USA. *Journal of Petrology* **46**, 859–891.

Peacock, S. M. (1990). Fluid processes in subduction zones. *Science* **248**, 329–337.

Philpotts, A. R., Carrol, M. & Hill, J. M. (1996). Crystal-mush compaction and the origin of pegmatitic segregation sheets in a thick flood-basalt flow in the Mesozoic Hartford Basin, Connecticut. *Journal of Petrology* **37**, 811–836.

Plank, T. & Langmuir, C. H. (1998). The chemical composition of subducting sediment and its consequences for the crust and mantle. *Chemical Geology* **145**, 325–394.

Rabinowicz, M., Genthon, P., Ceuleneer, G. & Hillairet, M. (2001). Compaction in a mantle mush with high melt concentrations and

the generation of magma chambers. *Earth and Planetary Science Letters* **188**, 313–328.

Reid, M. R., Coath, C. D., Harrison, M. T. & McKeegan, K. D. (1997). Prolonged residence times for the youngest rhyolites associated with Long Valley Caldera: ^{230}Th–^{238}U ion microprobe dating of young zircons. *Earth and Planetary Science Letters* **150**, 27–39.

Ribeiro-Lauret, M. (2008). Adakitic magmas: amphibole composition and geobarometric constraints. *Geological Society of America, Abstracts with Programs* **40**, 249.

Schmidt, M. W., Dardon, A., Vannucci, R. & Chazo, R. (2004). The dependence of Nb and Ta rutile–melt partitioning on melt composition and Nb/Ta fractionation during subduction processes. *Earth and Planetary Science Letters* **226**, 415–432.

Shirley, D. N. (1986). Compaction in igneous cumulates. *Journal of Geology* **94**, 795–809.

Sisson, T. W. & Bacon, C. R. (1999). Gas-driven filter pressing in magmas. *Geology* **27**, 613–616.

Spikings, R. A., Winkler, T. W., Hughes, R. A. & Handler, R. (2005). Thermochronology of allochthonous terranes in Ecuador: Unravelling the accretionary and post-accretionary history of the Northern Andes. *Tectonophysics* **399**, 195–220.

Streck, M. J. & Grunder, A. (2007). Phenocryst-poor rhyolites of bimodal, tholeiitic provinces: the Rattlesnake Tuff and implications for mush extraction models. *Bulletin of Volcanology* **70**, 385–401.

Sun, S.-S. & McDonough, W. F. (1989). Chemical and isotopic systematics of ocean arc basalts: implications for mantle composition and processes. In: Saunders, A. D. & Norry, M. J. (eds) *Magmatism in the Ocean Basins. Geological Society, London, Special Publications* **42**, 313–345.

Taboada, A. *et al.* (2000). Geodynamics of the northern Andes: Subductions and intracontinental deformation (Colombia). *Tectonics* **19**, 787–813.

Tera, F. & Wasserburg, G. J. (1974). U–Th–Pb systematics on lunar rocks and inferences about lunar evolution and the age of the moon. *Proceedings of the 5th Lunar Science Conference. Geochimica et Cosmochimica Acta, Supplement 5, Vol. 2* 1571–1599.

Thompson, G., Malpas, J. & Smith, I. (2001). Origin of oceanic phonolites by crystal fractionation and the problem of the Daly gap: An example from Rarotonga. *Contributions to Mineralogy and Petrology* **142**, 336–346.

Tiepolo, M., Bottazzi, P., Foley, S. F., Oberti, R., Vannucci, R. & Zanetti, A. (2000). Fractionation of Nb and Ta from Zr and Hf at mantle depths: the role of titanian pargasite and kaersutite. *Journal of Petrology* **42**, 221–232.

Turner, S. P., George, R. M., Evans, P. J., Hawkesworth, C. J. & Zellmer, G. F. (2000). Timescales of magma formation, ascent and storage beneath subduction-zone volcanoes. *Philosophical Transactions of the Royal Society of London* **358**, 1443–1464.

Vazquez, J. A. & Reid, M. R. (2004). Probing the accumulation history of the voluminous Toba magma. *Science* **305**, 991–994.

Vigneresse, J. L. & Clemens, J. D. (2000). Granitic magma ascent and emplacement: neither diapirism nor neutral buoyancy. In: Vendeville, B. C., Mart, Y. & Vigneresse, J.-L. (eds) *Salt, Shale and Igneous Diapirs. Geological Society, London, Special Publications* **174**, 1–19.

Volpe, A. M. (1992). ^{238}U–^{230}Th–^{226}Ra disequilibrium in young Mt. Shasta andesites and dacites. *Journal of Volcanology and Geothermal Research* **53**, 227–238.

Watts, R. B., de Silva, S. L., Jimenez de Rios, G. & Croudace, I. (1999). Effusive eruption of viscous silicic magma triggered and driven by recharge; a case study of the Cerro Chascon–Runto Jarita Dome Complex in Southwest Bolivia. *Bulletin of Volcanology* **61**, 241–264.

White, W. M., McBirney, A. R. & Duncan, R. A. (1993). Petrology and geochemistry of the Galapagos Islands: portrait of a pathological mantle plume. *Journal of Geophysical Research* **98**, 19533–19563.

Wolf, T. (1878). *Memoria sobre el Cotopaxi y su última erupción acaecida el 26 de junio de 1877*, Imprenta El Comercio, Guayaquil, p. 4.

Wolff, J. A., Balsley, S. D. & Gregory, R. T. (2002). Oxygen isotope disequilibrium between quartz and sanidine from the Bandelier Tuff, New Mexico, consistent with a short residence time of phenocrysts in rhyolitic magma. *Journal of Volcanolology and Geothermal Research* **116**, 119–135.

Zheng, Y. F. (1993). Calculation of oxygen isotope fractionation in hydroxyl-bearing silicates. *Earth and Planetary Science Letters* **120**, 247–263.

APPENDIX

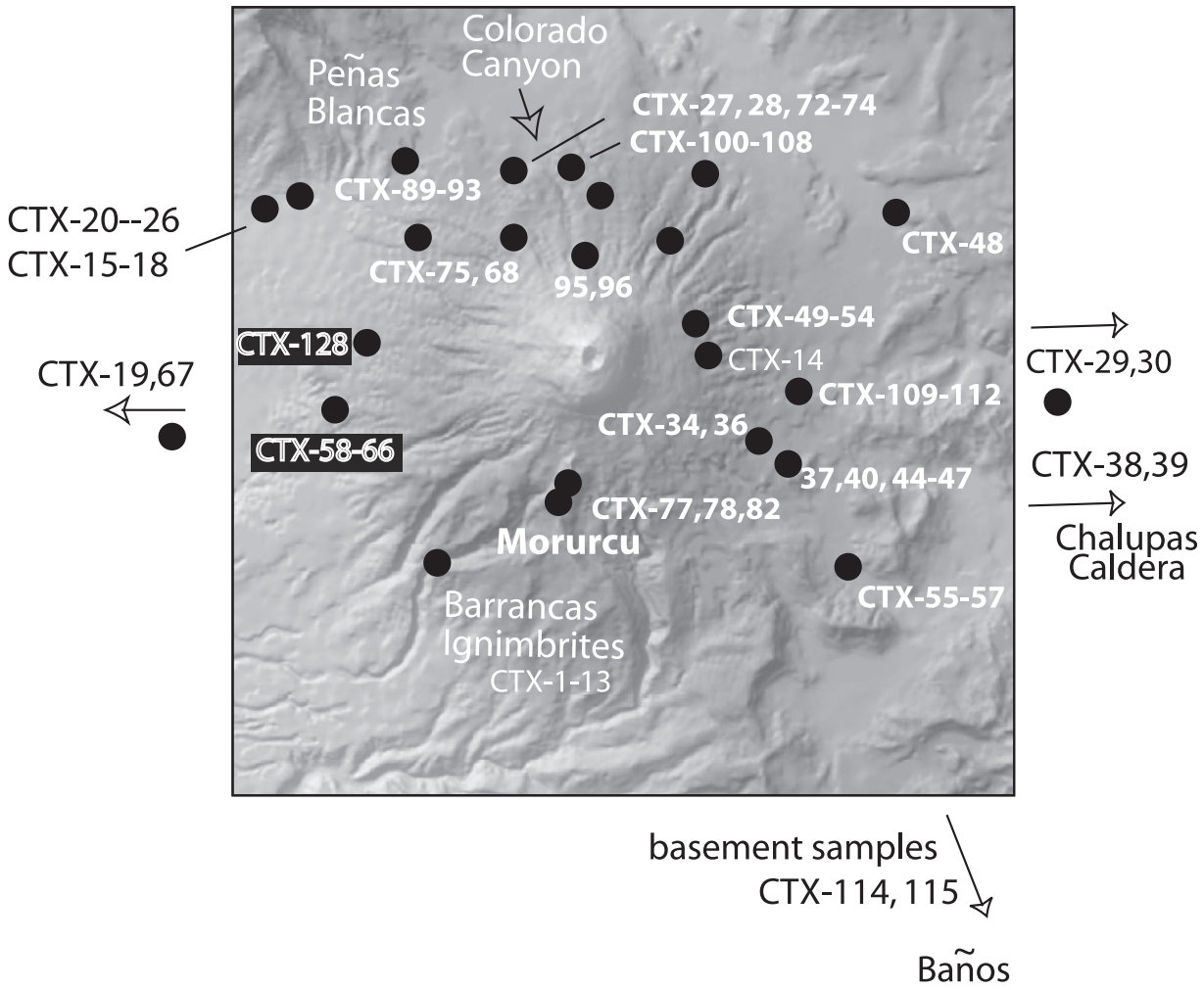

Fig. A1. Shaded relief map of the Cotopaxi region, showing locations of samples used in this study. Image from Hall & Mothes (2008).

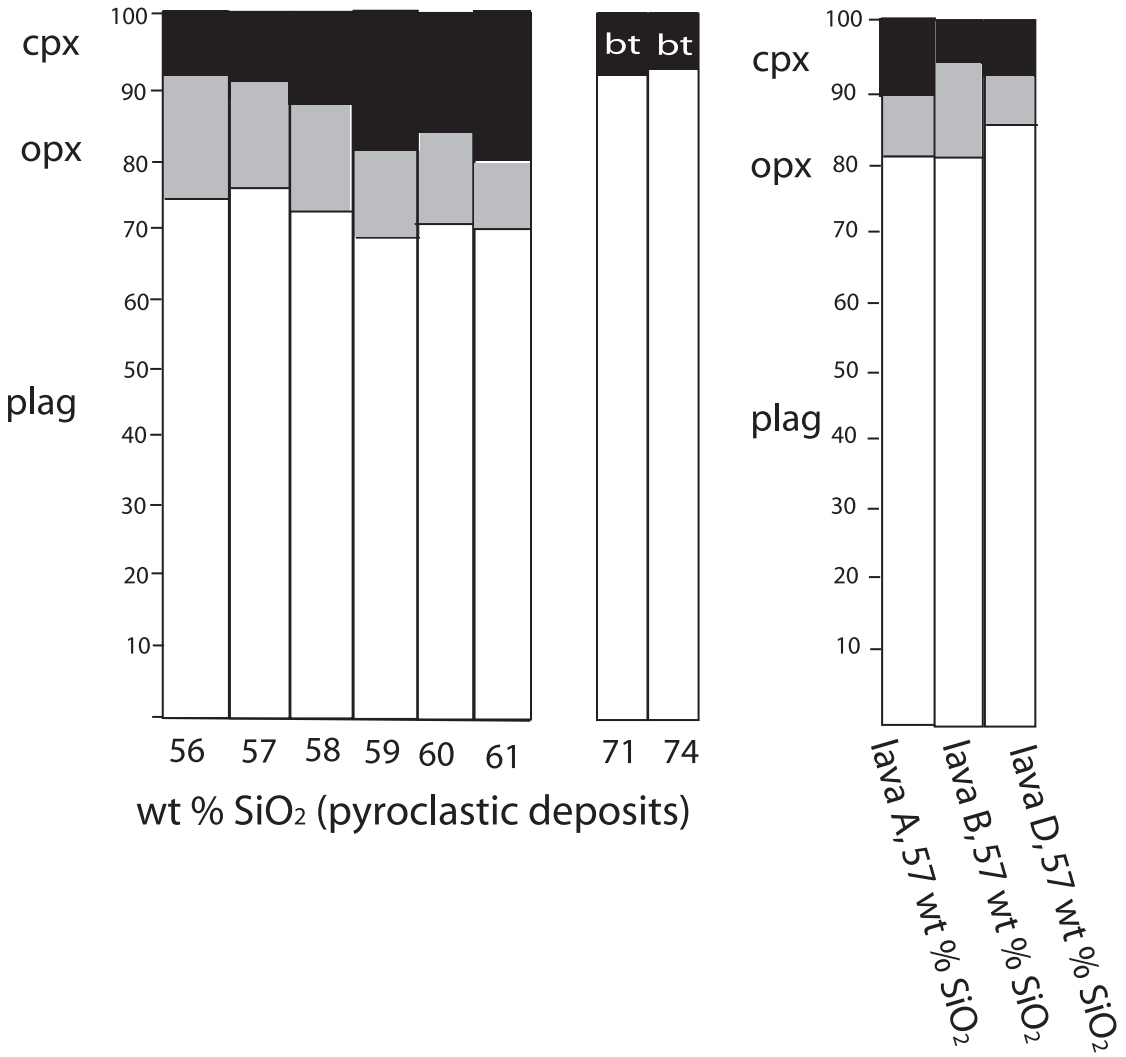

Fig. A2. Diagram showing average modal abundance of crystals versus wt. % SiO_2 for pyroclastic deposits and lava flows A, B and D.

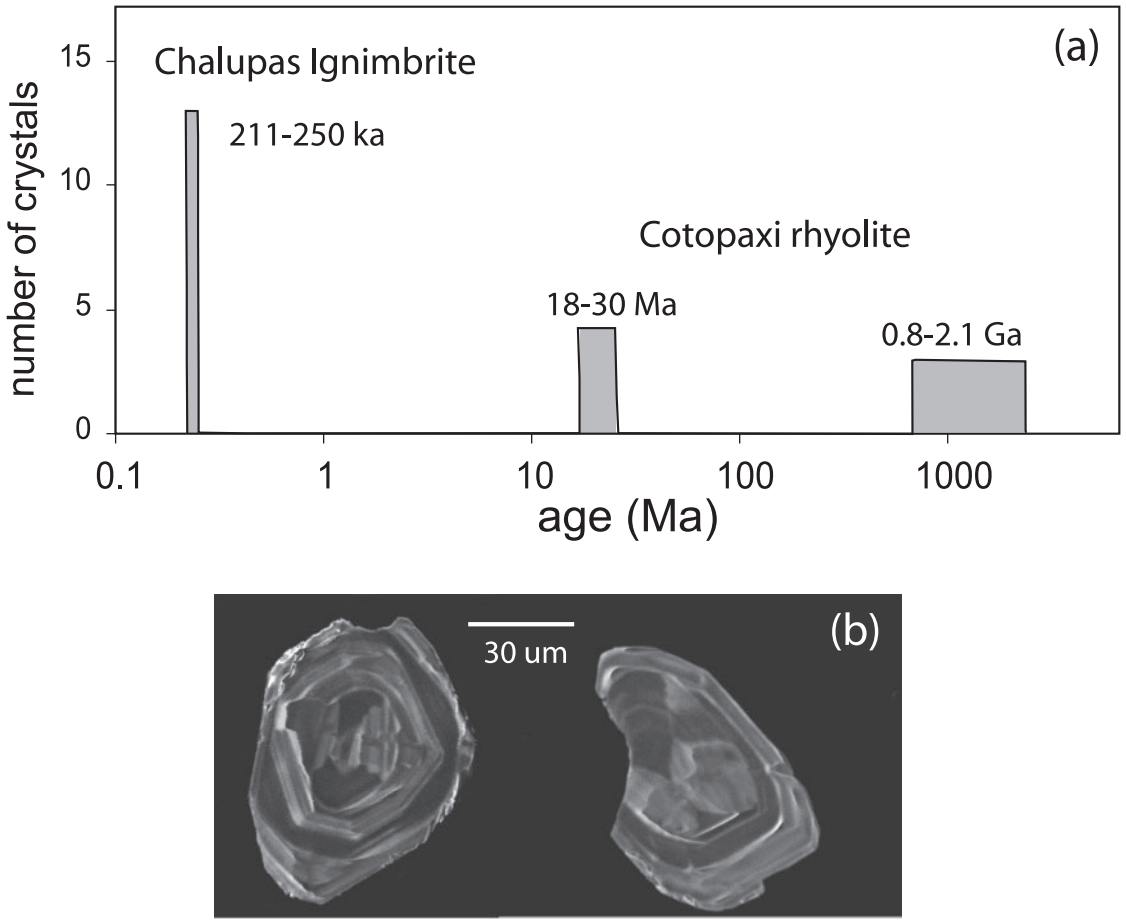

Fig. A3. (a) Illustrative diagram showing the general relationship between the ages of the seven Cotopaxi rhyolite zircon crystals and the zircon crystals from the Chalupas Caldera Ignimbrite. The width of each bar signifies the approximate age range. Actual ages were determined using Tera–Wasserburg diagrams (Tera & Wasserburg, 1974). (b) Cathodoluminescence images of zircon crystals from the Chalupas Caldera Ignimbrite (left) and one of the Cotopaxi rhyolites (CTX 19).

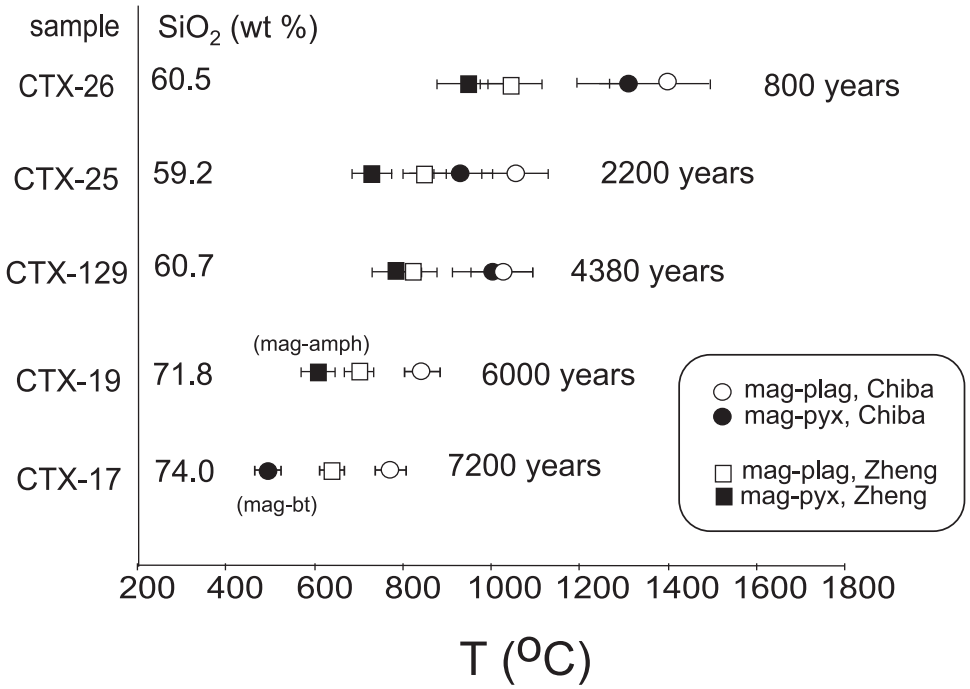

Fig. A4. Oxygen isotope temperature data for a subset of the Cotopaxi samples. Temperatures are calculated using fractionation factors from Chiba *et al.* (1989) and Zheng (1993). Mag-amphibole and mag-biotite data for the rhyolites are from Bottinga & Javoy (2000). Eruption ages are listed to the right of the temperature data.